Widespread slab melting in modern subduction zones

Martijn Klaver[1]*, Gene Yogodzinski[2], Capucine Albert[1], Michal Camejo-Harry[3], Marlina Elburg[4], Kaj Hoernle[5], Colin Macpherson[6], Geoff Nowell[6], Tracy Rushmer[7], Helen Williams[6,8], and Marc-Alban Millet[1]
[1]School of Earth and Environmental Science, Cardiff University, Main Building, Park Place, Cardiff CF10 3AT, United Kingdom
[2]School of Earth, Ocean, and Environment, University of South Carolina, Columbia, SC 29208-3402, United States
[3]Department of Earth Sciences, University of Oxford South Parks Road, Oxford OX1 3AN, United Kingdom
[4]Department of Geology, University of Johannesburg, PO Box 524, Auckland Park 2006, South Africa
[5]GEOMAR Helmholtz Centre for Ocean Research Kiel, Wischhofstrasse 1-3, 24148 Kiel, Germany
[6]Department of Earth Sciences, Durham University, South Road, Durham DH1 3LE, United Kingdom
[7]Faculty of Science and Engineering, Macquarie University, 7 Wally's Walk (E6B) Level One, NSW 2109, Australia
[8]Department of Earth Sciences, University of Cambridge, Cambridge CB2 3EQ, United Kingdom
*Corresponding author: klaverm@cardiff.ac.uk

ABSTRACT
It is still a matter of intense debate to what extent partial melting of the subducting slab contributes to arc magmatism in modern subduction zones. In particular, it is difficult to differentiate between silicate melts formed by partial melting of the slab, and aqueous fluids released during subsolidus dehydration as the main medium for slab-to-mantle wedge mass transfer. Here we use $\delta^{49/47}$Ti (the deviation in ^{49}Ti/^{47}Ti of a sample to the OL-Ti reference material) as a robust geochemical tracer of slab melting. Hydrous partial melting of subducted oceanic crust and the superjacent sedimentary layer produces silicic melts in equilibrium with residual rutile. Modelling shows that such silicic slab melts have notably higher $\delta^{49/47}$Ti (+0.24±0.06‰) than their protolith due to the strong preference of rutile for the lighter isotopes of Ti. In contrast, even highly saline fluids cannot carry Ti from the slab and hence hydrous peridotite partial melts have $\delta^{49/47}$Ti similar to mid-ocean ridge basalts (MORB; ca. 0‰).

Primitive (Mg# ≥60) arc lavas from eight subduction zones that are unaffected by fractional crystallisation of Fe-Ti oxides show a more than tenfold larger variation in $\delta^{49/47}$Ti than found in MORB. In particular, primitive arc lavas display a striking correlation between SiO_2 content and $\delta^{49/47}$Ti that ranges from island arc basalts overlapping with MORB, to primitive rhyodacites with $\delta^{49/47}$Ti up to 0.26‰ erupted in the western Aleutian arc. The elevated $\delta^{49/47}$Ti of these primitive arc lavas provides conclusive evidence for partial melts of the slab as a key medium for mass transfer in subduction zones. The Aleutian rhyodacites represent a rare example of slab melts that have traversed the mantle wedge with minimal modification. More commonly, slab melts interact with the mantle wedge to form an array of primary arc magmas that are a blend of slab- and peridotite-derived melt. We identify primitive arc lavas with a clearly resolvable slab melt signature in all eight subduction zone localities, confirming that slab melting is prevalent in modern subduction zones.

Keywords: Slab melting; Titanium isotopes; Rutile; Subduction zone; Aleutian arc

Highlights

- Global primitive arc lavas (Mg# ≥60) display notable $\delta^{49/47}$Ti heterogeneity
- Residual rutile imposes high $\delta^{49/47}$Ti of 0.24±0.06‰ on hydrous, silicic slab melts
- Primitive Aleutian rhyodacites have the same $\delta^{49/47}$Ti as predicted for slab melts
- A variably diluted signature of slab melts is found in all eight subduction zones
- A slab melt component is required to generate silicic primitive arc lavas

1. Introduction

Subduction zones are a nexus of geochemical cycles and link the crust, hydrosphere, atmosphere, and Earth's mantle. Mass transfer from subducting slabs is a likely trigger for partial melting of the overlying mantle wedge, giving rise to arc lavas with a ubiquitous geochemical signature of subducted oceanic crust and its sedimentary cover (e.g., Gill, 1981; Tera et al., 1986; White and Dupré, 1986; Plank and Langmuir, 1993; Elliott et al., 1997). Despite the key role in modulating the composition of the continental crust, deep mantle, and Earth's surface habitat, the mechanisms of mass transfer in subduction zones are still not well understood (Spandler and Pirard, 2013; Keppler, 2017; Nielsen and Marschall, 2017; Hernández-Uribe et al., 2020; Klaver et al., 2020). A persistent question is to what extent the top of the subducting slab melts in modern subduction zones. Melts are an efficient medium to mobilise trace elements and volatiles from the slab (e.g., Johnson and Plank, 1999; Hermann et al., 2006), and the latest generation of slab thermal models (Syracuse et al., 2010; van Keken et al., 2011; van Keken et al., 2018) and geochemical slab-top thermometers (Cooper et al., 2012) suggest that the hydrous solidus of sediments and altered oceanic crust can be reached in most modern subduction zones. Conversely, saline aqueous fluids might also be capable of carrying a significant budget of trace elements to the mantle wedge source of arc magmas without the need to invoke slab melting (Tatsumi, 1989; Keppler, 2017; Rustioni et al., 2021).

The trace element and radiogenic isotopic signature of primitive arc lavas unquestionably supports slab-to-mantle wedge mass transfer, but does not provide a conclusive discrimination between slab melting and transport by saline fluids (cf. Rustioni et al., 2021; Li et al., 2022; Turner and Langmuir, 2022b). For instance, either model explains the characteristic relative depletion in Ti, Nb, and Ta displayed by primitive arc lavas. In the sediment melting scenario, this depletion is imposed by the accessory mineral rutile (TiO_2) present in the residue during hydrous melting of eclogite-facies slab lithologies (e.g., Ryerson and Watson, 1987; Yogodzinski et al., 1995; Elliott et al., 1997), whereas in the saline fluid model the relative depletion in Ti, Nb, and Ta results from the negligible solubility of these elements in fluids. Here, we demonstrate that the isotopic composition of Ti in primitive arc lavas is a uniquely diagnostic tracer of the presence of a slab melt component in primitive arc magmas. This approach hinges on the distinct bonding environment of Ti in Fe-Ti oxides. Rutile has a strong preference for the lighter isotopes of Ti compared to silicate minerals and melts (Aarons et al., 2021; Hoare et al., 2022; Rzehak et al., 2022). As a result, partial melts in equilibrium with residual rutile will display the characteristic relative depletion in Ti, Nb, and Ta, as well as distinctly heavier Ti isotope compositions than their protolith. In contrast, experimental studies indicate that aqueous fluids cannot mobilise Ti even at high salinities (e.g., Kessel et al., 2005a; Keppler, 2017; Rustioni et al., 2021), and as rutile is not a stable residual phase during hydrous peridotite melting (Grove et al., 2006; Till et al., 2012), mass transfer by saline fluids alone does not have the capability to impose a distinct Ti isotope signature on primitive arc lavas.

We test this hypothesis by combining quantitative Ti isotope fractionation modelling of slab melting with high-precision Ti isotope composition measurements of a comprehensive suite of global primitive arc lavas. This shows that slab melting occurs in all eight subduction zones for which Ti isotope data are available, irrespective of slab age and temperature, and therefore is a widespread feature of modern subduction zones.

2. Samples and analytical techniques

We present new Ti isotope composition data for 52 extrusive volcanic samples from six subduction zone localities. These comprise the Aegean arc (Nisyros and Santorini), Aleutian arc (Adak and dredge samples from the Komandorsky Straits and Western Cones area), Lesser Antilles arc (Bequia, Grenada, Saba, and St. Vincent), Philippines arc (Surigao Peninsula, Mindanao), Solander Islands (New Zealand), and Cook Island (Austral Volcanic Zone, Chile). A detailed description of these localities and the samples is provided in the supplementary material. The new data greatly expand on previously published data (26 samples) for arc lavas from the New Britain arc (Millet and Dauphas, 2014), Mariana arc (Millet et al., 2016), Kermadec arc (Monowai; Hoare et al., 2020), and Aegean arc (Santorini, Kos; Hoare et al., 2020; Greber et al., 2021). Taken together, these localities cover a wide range of subduction zone parameters such as the age of subducted crust (10 to ca. 200 Ma), slab dip (30–70°), and subduction angle (straight versus oblique; see supplementary

Table S4). All samples have a minimum of major- and trace element characterisation, in most cases complemented with radiogenic isotope data (compiled in supplementary Dataset 2).

For the selection of the new samples, emphasis was placed on primitive lavas that are least affected by magmatic differentiation. We use Mg# (molar 100×Mg/[Mg+Fe]) as discriminant and designate samples with Mg# ≥60 as primitive, and samples with Mg# <60 as evolved. In addition, we specifically targeted primitive arc lavas with a geochemical signature often ascribed to slab melts, such as elevated Sr/Y, fractionated rare earth element patterns, and high SiO_2 content (e.g., Defant and Drummond, 1990). Although such primitive andesites, dacites, and rhyodacites are a volumetrically minor fraction of global arc magmas (Kelemen et al., 2014), they are well-suited to test the sensitivity of Ti isotopes to slab melting. In particular, we include seafloor rhyodacites with high Mg# (64–73) erupted on thin oceanic crust in the western Aleutian arc, which are proposed to be nearly unmodified melts of the subducting Pacific oceanic crust (Yogodzinski et al., 2015; Yogodzinski et al., 2017).

Titanium isotope composition measurements were carried out following a well-established protocol described in detail elsewhere (e.g., Millet and Dauphas, 2014; Hoare et al., 2020; Klaver et al., 2021). Briefly, aliquots of dissolved sample corresponding to ca. 5 µg Ti were equilibrated with a ^{47}Ti–^{49}Ti double spike prior to Ti purification with Eichrom DGA resin. Measurements were performed using a ThermoScientific Neptune Plus (at Durham University) and Nu Plasma II (at Cardiff University) multi-collector inductively-coupled plasma mass spectrometer (MC-ICP-MS) operated in medium resolution mode. Titanium isotope composition data are reported in the conventional delta-notation relative the Origins Laboratory Ti reference material (OL-Ti) as $\delta^{49/47}Ti_{OL\text{-}Ti}$ (hereafter abbreviated to $\delta^{49/47}Ti$). Repeat measurements of geological and Ti solution reference materials indicates an intermediate precision of 0.020‰ (2s) for the individual measurements made in Durham (Millet et al., 2016) and 0.030‰ (2s) for those made in Cardiff (supplementary Figure S3). For most samples measured in Cardiff, 2–4 repeat measurements were made (see supplementary Dataset 2). See the supplementary material for more discussion of measurement uncertainties.

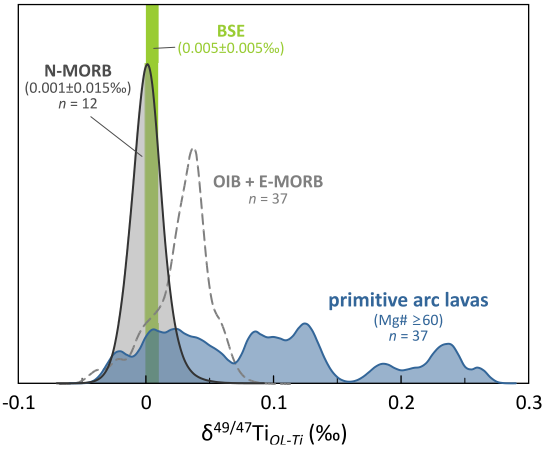

Figure 1. *Kernel density diagram for primitive arc lavas (Mg# ≥60) compared to normal mid ocean ridge basalts (N-MORB; Millet et al., 2016; Deng et al., 2018) and ocean island basalts (OIB) pus enriched MORB (Millet et al., 2016; Deng et al., 2018; Deng et al., 2019; Hoare et al., 2020; Deng et al., 2023). See supplementary Dataset 2 for all data. The field for the bulk silicate Earth (BSE) is from Millet et al. (2016). Primitive arc lavas have $\delta^{49/47}Ti$ that extends to higher values than MORB.*

3. Results

The primitive arc lavas (whole rock Mg# ≥60) in this study vary in major element composition from (picritic) basalts with 46 wt.% SiO_2 and up to 15.5 wt.% MgO (e.g., St. Vincent, Lesser Antilles arc) to high-Mg# rhyodacites (70 wt.% SiO_2, 2.1 wt.% MgO) erupted as submarine lavas on oceanic crust in the western Aleutian arc. Despite the large range in silica content, their high Mg# indicates that these arc lavas are primitive melts that are in or very close to equilibrium with mantle olivine and/or orthopyroxene. As shown in Figure 1,

primitive arc lavas display notably heterogeneous $\delta^{49/47}$Ti (ca. 0.3‰ variation) compared to normal mid ocean ridge basalts (N-MORB), which have homogeneous $\delta^{49/47}$Ti of 0.001±0.015‰ (Millet et al., 2016; Deng et al., 2018). Basaltic primitive arc lavas overlap in $\delta^{49/47}$Ti with N-MORB but more silica-rich varieties have progressively higher $\delta^{49/47}$Ti. The high-Mg# rhyodacites from the Aleutian arc have the most extreme $\delta^{49/47}$Ti at 0.21–0.26‰, but also high-Mg# andesites from the Aegean arc, Philippines arc, Solander Islands, and Cook Island have $\delta^{49/47}$Ti clearly elevated relative to N-MORB.

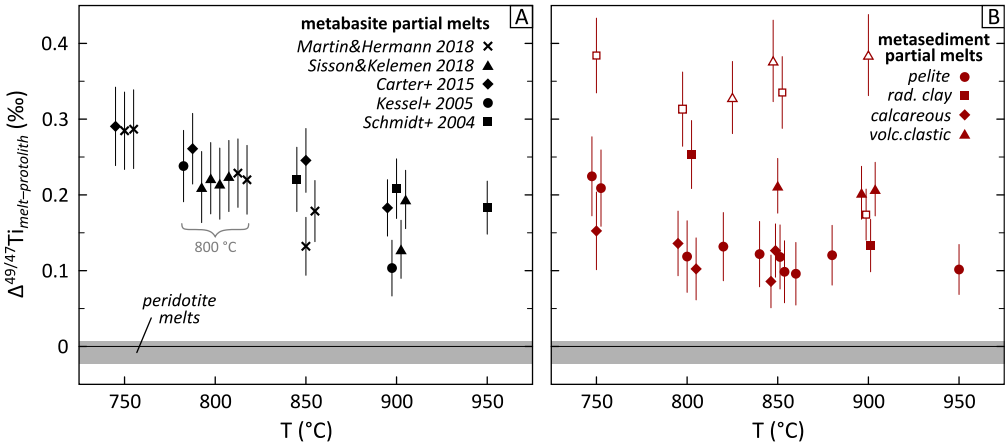

Figure 2. *The modelled magnitude of Ti isotope fractionation during hydrous melting of (altered) MORB (A) and various sediment lithologies (B) at 2.6–6 GPa, expressed as* $\Delta^{49/47}Ti_{melt-protolith}$*, which is the difference in* $\delta^{49/47}Ti$ *between the partial melt and the protolith. Experimental studies (Schmidt et al., 2004; Kessel et al., 2005b; Skora and Blundy, 2010; Martindale et al., 2013; Carter et al., 2015; Mann and Schmidt, 2015; Skora et al., 2015; Martin and Hermann, 2018; Sisson and Kelemen, 2018) yield the phase proportions and Ti content of the partial melt and residual minerals after which* $\Delta^{49/47}Ti_{melt-protolith}$ *is calculated by isotopic mass balance using Ti isotope mineral–melt fractionation factors (supplementary Tables S1 and 2). Rutile is invariably present as a residual phase during hydrous melting of metabasite and metasediment, which imposes an isotopically heavy Ti isotope signature on the partial melt. Some symbols are shifted slightly to higher or lower temperature (≤5 °C unless indicated) to prevent cluttering of the datapoints. The open symbols in panel B denote experiments where both titanomagnetite (≥0.5 wt.% abundance) and rutile are present as residual phase. The grey field shows the Ti isotope fractionation of 2–25% anhydrous partial melts of a fertile peridotite at 1–2.5 GPa. See supplementary material for a detailed description of the modelling approach and parameters used; the melting models are provided in supplementary Dataset 1. A corresponding figure for the fractionation of the melting residua relative to the protolith (*$\Delta^{49/47}Ti_{residue-protolith}$*) is provided in the supplementary material (Figure S2).*

4. Modelling Ti isotope fractionation during slab melting

The contrasting bonding environment of Ti in Fe-Ti oxides compared to silicate minerals and melts is the fundamental parameter that introduces Ti isotope heterogeneity during magmatic processes (e.g., Millet et al., 2016; Deng et al., 2019; Hoare et al., 2020). Titanium isotope fractionation between silicate minerals (e.g., pyroxene, garnet) and silicate melt is negligible and, as a result, partial melting of peridotite produces melts with essentially the same $\delta^{49/47}$Ti as their protolith (Figure 2; Hoare et al., 2022). Conversely, Fe-Ti oxide minerals, notably rutile, have a strong preference for the lighter isotopes of Ti relative to silicates (Aarons et al., 2021; Hoare et al., 2022; Rzehak et al., 2022). As a result, the presence of rutile in the residue during partial melting will aid the retention of Ti and impose an isotopically heavy Ti isotope signature on the partial melt.

Rutile is a stable residual phase during hydrous partial melting of eclogite-facies metabasite and metasediment due to the low solubility of TiO_2 in the silicic partial melts produced at 750–1000 °C (Ryerson and Watson, 1987; Gaetani et al., 2008; Xiong et al., 2009). We use experimentally determined melting reactions of such slab lithologies coupled with mineral–melt Ti isotope fractionation factors to model the magnitude of Ti isotope fractionation that occurs during melting in the presence of residual rutile. Rutile is the main repository of Ti in the melting residua of metabasite and metasediment, and the rutile–melt Ti isotope

fractionation factor therefore exerts the dominant control on the magnitude of Ti isotope fractionation during melting. We employ an average rutile–melt Ti isotope fractionation factor of $10^3 \ln\alpha_{rt-melt} = -0.444 \pm 0.028 \times 10^6/T^2$ compiled from two recent studies (Hoare et al., 2022; Rzehak et al., 2022). The difference in Ti isotope composition between the partial melt and the protolith ($\Delta^{49/47}Ti_{melt-protolith}$) can then be calculated through isotopic mass balance as described in detail in the supplementary material. Subsequently, the absolute $\delta^{49/47}Ti$ of slab melts can be derived by adding $\Delta^{49/47}Ti_{melt-protolith}$ as shown in Figure 2 to the $\delta^{49/47}Ti$ of the protolith ($\delta^{49/47}Ti_{slab\ melt} = \Delta^{49/47}Ti_{melt-protolith} + \delta^{49/47}Ti_{protolith}$).

The water-saturated solidus of eclogite with a composition akin to pristine to altered MORB (0–1.0 wt.% K_2O, 1.2–2.0 wt.% TiO_2) at sub-arc depths (2.6-4.5 GPa) lies between 750 and 800 °C (Schmidt et al., 2004; Kessel et al., 2005b; Carter et al., 2015; Martin and Hermann, 2018; Sisson and Kelemen, 2018). These studies find rutile as a residual phase up to at least 900 °C or 25% melting. As a result of the residual rutile, hydrous, silicic metabasite partial melts (73–79 wt.% SiO_2 on an anhydrous basis) have notably higher $\delta^{49/47}Ti$ than their protolith, in clear contrast with the negligible Ti isotope fractionation during partial melting of rutile-free peridotite (Figure 2a). Metabasite melts formed at 750–800 °C show the largest Ti isotope fractionation ($\Delta^{49/47}Ti_{melt-protolith}$ = 0.21–0.29‰; Figure 2a). At higher temperature, the diminishing proportion of rutile in the residue leads to progressively lower $\Delta^{49/47}Ti_{melt-protolith}$. The MORB protolith of the metabasite has $\delta^{49/47}Ti$ around zero (Figure 1; Millet et al., 2016; Deng et al., 2018); hence the absolute $\delta^{49/47}Ti$ of metabasite partial melts at 750–800 °C is 0.24±0.06‰.

Low-degree hydrous partial melts of eclogite-facies metasediments at 750–950 °C and 3–6 GPa are also in equilibrium with residual rutile (Skora and Blundy, 2010; Martindale et al., 2013; Mann and Schmidt, 2015; Skora et al., 2015) and therefore have higher $\delta^{49/47}Ti$ than their protolith (Figure 2b), unlike what was assumed by Kommescher et al. (2023). Given the lower TiO_2 content of the sedimentary protoliths, the proportion of rutile in the residue is generally smaller and the Ti isotope fractionation effect is more subdued compared to metabasite melting. In several cases, however, titanomagnetite joins rutile as a residual phase. Titanomagnetite has an even stronger preference for the lighter isotopes of Ti than rutile (Hoare et al., 2022) and hence its presence leads to higher $\Delta^{49/47}Ti_{melt-protolith}$ (0.3–0.4‰; Figure 2b). As a result, metasediment partial melts have highly variable $\Delta^{49/47}Ti_{melt-protolith}$, but are always positively fractionated relative to their protolith. Modern terrigenous sediments have $\delta^{49/47}Ti$ in the range of 0.16–0.24‰ (Greber et al., 2017; Klaver et al., 2021), meaning that hydrous metasediment partial melts have $\delta^{49/47}Ti$ ranging from 0.25‰ up to 0.6‰.

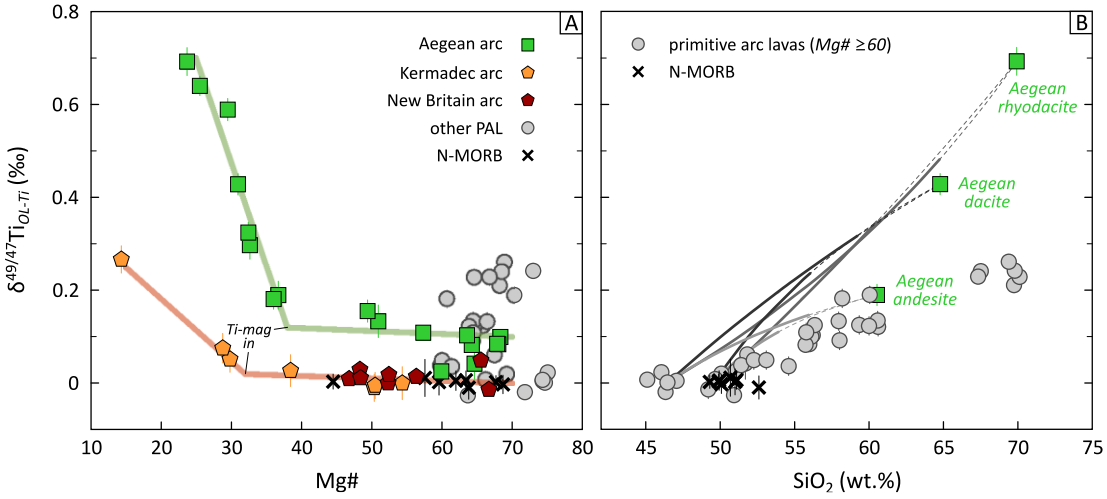

Figure 3. *Effects of magmatic differentiation on the Ti isotope composition of arc lavas. (A) Fractional crystallization of isotopically light titanomagnetite (Ti-mag) drives arc lavas to high $\delta^{49/47}Ti$. Two arc differentiation suites are shown: a tholeiitic Kermadec and New Britain arcs trend, and a calc-alkaline trend displayed by Santorini lavas (Aegean arc). Both suites show a clear inflection in $\delta^{49/47}Ti$ upon saturation of the melt with titanomagnetite at Mg# 30–40. At higher Mg#, fractional crystallization of silicate minerals has negligible effect on $\delta^{49/47}Ti$ and hence primitive arc lavas (PAL; Mg# ≥60) retain a primary Ti isotope signature.*

(B) Titanium isotope effects of magma mixing. Three sets of mixing lines are shown between primitive lavas (St. Vincent picrite RSV52, New Britain basalt 116852-5) and either evolved andesite (AAS-036), dacite (AAS-041), or rhyodacite (AAS-033) from Santorini (Aegean arc). The mixing lines are dashed where Mg# <60. Magma mixing cannot account for the $\delta^{49/47}$Ti variation seen in global primitive arc lavas.

5. Discussion

5.1. Negligible influence of magmatic differentiation on $\delta^{49/47}$Ti of primitive arc lavas

Differentiation of arc magmas in the crust modifies their composition and can obscure a mantle source signature. In case of Ti, magma mixing and fractional crystallization cause large $\delta^{49/47}$Ti variation in evolved arc lavas (Millet et al., 2016; Hoare et al., 2020; Greber et al., 2021). Several lines of evidence confirm, however, that the variations recorded in our primitive arc lavas represent a primary feature of their source rather result from magmatic differentiation. The removal of isotopically light Fe-Ti oxides, mainly titanomagnetite, during fractional crystallization drives arc magmas to higher $\delta^{49/47}$Ti (Deng et al., 2019; Hoare et al., 2020; Hoare et al., 2022) and evolved, low-Mg# rhyodacites from the Aegean arc display $\delta^{49/47}$Ti up to 0.7‰ (Figure 3a). Hoare et al. (2020) found that the saturation point of titanomagnetite may be dependent on the water content of arc magmas but generally occurs around Mg# 30–40. The onset of titanomagnetite fractionation causes a notable inflection in both TiO_2 content and $\delta^{49/47}$Ti versus Mg# (Figure 3a; Hoare et al., 2022). At higher Mg#, Ti is incompatible with only a small fraction hosted in clinopyroxene during fractional crystallization, which does not cause significant Ti isotope fractionation (Figure 3a). As a result, $\delta^{49/47}$Ti of primitive arc lavas (Mg# ≥60) is not affected by low-pressure fractional crystallization of Fe-Ti oxides.

Crystallisation of garnet at the base of thick crust or in the upper mantle is another mechanism that can generate silicic magmas with a geochemical signature similar to slab melts (e.g., high Sr/Y; Defant and Drummond, 1990), as proposed for instance by Macpherson et al. (2006). High-pressure fractional crystallisation, however, cannot explain the high $\delta^{49/47}$Ti as garnet, like other silicate minerals (see supplementary Figure S1), does not fractionate Ti isotopes relative to the melt. Furthermore, experimental studies indicate that, just as found for low-pressure fractional crystallisation (Figure 3a), Fe-Ti oxides are absent in early stages of high-pressure crystallisation (Alonso-Perez et al., 2009; Coldwell et al., 2011) and thus cannot drive an increase in $\delta^{49/47}$Ti at Mg# ≥60.

The high Mg# of primitive arc lavas also precludes significant modification by mixing with evolved magmas with low Mg# and elevated $\delta^{49/47}$Ti (Figure 3b). Binary mixing between a basaltic components with $\delta^{49/47}$Ti of ca. 0‰ and an evolved Aegean arc andesite (61 wt.% SiO_2, $\delta^{49/47}$Ti = 0.19‰), dacite (65 wt.% SiO_2, $\delta^{49/47}$Ti = 0.43‰), or rhyodacite (70 wt.% SiO_2, $\delta^{49/47}$Ti = 0.69‰) forms a much steeper array in $\delta^{49/47}$Ti *versus* SiO_2 space than the primitive arc lavas (Figure 3b). Furthermore, andesites and dacites from Kos (Aegean arc) that formed through extensive hybridization of mafic and felsic melts may have similar $\delta^{49/47}$Ti to the primitive arc lavas, but they also have Mg# <60 (Greber et al., 2021). In general, there does not exist a mixing solution that can reproduce the combined SiO_2–$\delta^{49/47}$Ti signature of the primitive arc lavas at Mg# ≥60.

The primitive rhyodacites from western Aleutian arc with $\delta^{49/47}$Ti of 0.21–0.26‰ are the most extreme arc lavas in this study and therefore deserve special consideration. The absence of Fe-Ti oxide phenocrysts suggests that these magmas are undersaturated with respect to Fe-Ti oxides. In general, the geochemical variability of lavas from the western Aleutian arc is inconsistent with any plausible fractional crystallisation process, and the complete absence of evolved (Mg# <55) samples further attests to the negligible role that intracrustal differentiation plays in this locality (Yogodzinski et al., 2015). Extensive fractional crystallisation of hydrous basaltic magmas in the mantle wedge, including removal of a Fe-Ti oxide phase and concomitant Ti isotope fractionation, followed by re-equilibration with mantle wedge peridotite to re-establish Mg# ≥60 (Macpherson et al., 2006) is therefore also unlikely. Furthermore, in such a scenario it would be expected that a broad spectrum of primitive lavas ranging from basalts to rhyodacites are erupted, but only primitive rhyodacites are recovered from the Western Cones area and there is no trace of lavas with lower Mg# or SiO_2 (Yogodzinski et al., 2015). Hence, the unusual Ti isotope variation observed in the western Aleutian

rhyodacites and other primitive arc lavas in this study does not result from crustal processes but reflects a primary signature that informs on the mode of slab-to-mantle wedge mass transfer in subduction zones.

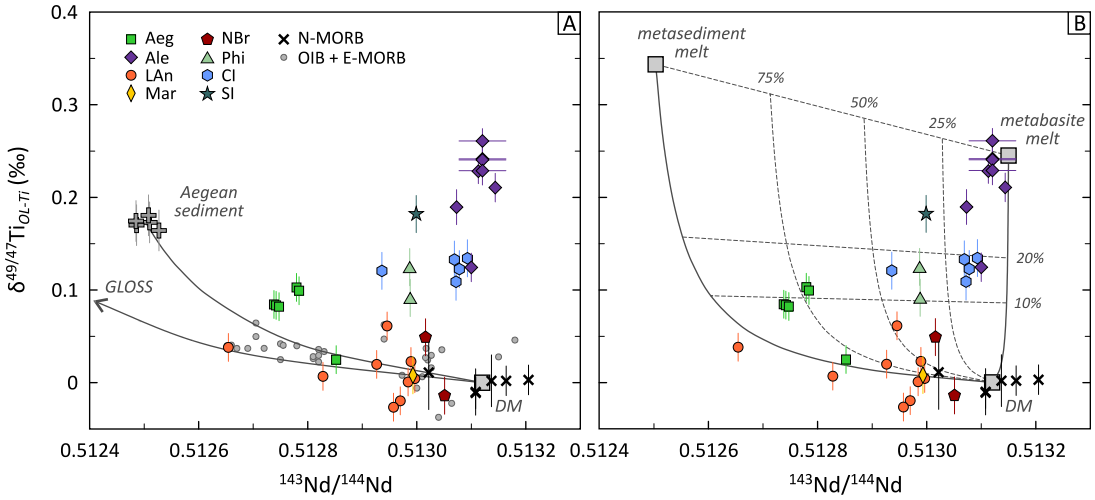

Figure 4. *Variation in $\delta^{49/47}Ti$ of primitive arc lavas (Mg# ≥60) versus $^{143}Nd/^{144}Nd$; see supplementary Dataset 2 for all data shown in the figure. (A) Model curves showing binary mixing between a depleted mantle (DM) source (0.05 wt.% TiO_2, 0.4 µg/g Nd) and bulk sediment subducting in the Aegean arc (Klaver et al., 2021) or global subducting sediment (GLOSS; Plank and Langmuir, 1998) with $\delta^{49/47}Ti$ estimated at 0.24‰ (i.e., the maximum of modern marine sediments; Greber et al., 2017). The compositions of N-MORB and OIB+E-MORB are shown for comparison – see Figure 1 for data sources. (B) Model curves for mixing between a depleted mantle (DM) source and hydrous partial melts of metabasite and metasediment. The composition of the metabasite partial melt ($\delta^{49/47}Ti$ = 0.24‰, 0.24 wt.% TiO_2) is the average $\Delta^{49/47}Ti_{melt-protolith}$ for metabasite at 750–800 °C (0.244‰; see Figure 2a) added to the average $\delta^{49/47}Ti$ of N-MORB (0.001‰; see Figure 1). The metasediment partial melt ($\delta^{49/47}Ti$ = 0.34‰, 0.17 wt.% TiO_2) is the average $\Delta^{49/47}Ti_{melt-protolith}$ for metasediment (without titanomagnetite) at 750–800 °C (0.171‰; see Figure 2b) added to the average $\delta^{49/47}Ti$ of sediment subducting in the Aegean arc (0.172‰; Klaver et al., 2021). Both metabasite and metasediment partial melt are assumed to have Ti/Nd of 55 (Martindale et al., 2013; Skora et al., 2015; Sisson and Kelemen, 2018). Aleutian arc rhyodacites for which no Nd isotope data are available are plotted at the average $^{143}Nd/^{144}Nd$ of similar samples from the Western Cones area where $^{143}Nd/^{144}Nd$ is homogeneous at 0.51312±0.00004. Sample location abbreviations: Aeg – Aegean arc; Ale – Aleutian arc; LAn – Lesser Antilles arc; Mar – Mariana arc; NBr – New Britain arc; Phi – Philippines arc; CI – Cook Island (Austral Volcanic Zone, Chile); SI – Solander Islands (New Zealand).*

5.2. Bulk addition of sediments

Recycled sediments form a key component of arc magmas and could contribute to the elevated $\delta^{49/47}Ti$ of primitive arc lavas. Phanerozoic marine sediments have higher $\delta^{49/47}Ti$ (0.16–0.24‰; Greber et al., 2017; Klaver et al., 2021) than N-MORB, but only barely reach the $\delta^{49/47}Ti$ of primitive rhyodacites from the Aleutian arc (Figure 4). We investigate the role of sediments by combining $\delta^{49/47}Ti$ with radiogenic Nd isotopes ($^{143}Nd/^{144}Nd$) that act as a sensitive proxy for recycled sediment. For the Aegean arc there are direct constraints on $\delta^{49/47}Ti$ of subducting sediments, which are homogeneous at 0.172±0.012‰ and have $^{143}Nd/^{144}Nd$ of 0.5125 (Klaver et al., 2021). Bulk mixing of depleted mantle wedge peridotite with Aegean sediment causes a rapid decrease in $^{143}Nd/^{144}Nd$ but only a subdued increase in $\delta^{49/47}Ti$ in the peridotite (Figure 4a). Mixing with sediment that has lower $^{143}Nd/^{144}Nd$, such as the global subducting sediment average (GLOSS; Plank and Langmuir, 1998), has an even smaller influence on $\delta^{49/47}Ti$. Hence, bulk mixing with subducting sediment can only cause a resolvable Ti isotope effect in primitive arc lavas with highly unradiogenic Nd isotope compositions. Moreover, partial melting of physical mixtures of sediment and mantle wedge peridotite, as proposed in the mélange model (e.g., Nielsen and Marschall, 2017), does not leave residual rutile

or another Fe-Ti oxide phase (Codillo et al., 2018), and is hence not accompanied by Ti isotope fractionation. Two samples from the Lesser Antilles arc and one from the Aegean arc with $^{143}Nd/^{144}Nd$ <0.5129 show combined Ti–Nd isotope compositions that can be consistent with bulk sediment mixing. A group of samples (predominantly from the Lesser Antilles) have $\delta^{49/47}Ti$ and $^{143}Nd/^{144}Nd$ similar to MORB, but the majority of the primitive arc lavas have rather radiogenic Nd isotope compositions ($^{143}Nd/^{144}Nd$ >0.5129) coupled with much higher $\delta^{49/47}Ti$ than sediment–peridotite mixtures, indicating that bulk sediment addition cannot account for the observed Ti isotope heterogeneity of primitive arc lavas.

5.3. Partial melts in equilibrium with rutile

The only viable agent that can impose elevated $\delta^{49/47}Ti$ on primitive arc lavas is a partial melt generated in the presence of residual rutile. The stability of rutile in a melting residue is an interplay between the Ti content of the protolith and the solubility of TiO_2 in the partial melt. Rutile solubility increases with temperature and is much higher in mafic melts than in silicic, alkali-rich melts (Ryerson and Watson, 1987; Gaetani et al., 2008; Xiong et al., 2009). As such, rutile is not a residual phase during melting of sediment–peridotite mixtures (mélanges) as the TiO_2 solubility in such high-temperature (>1200 °C) mafic partial melts exceeds the TiO_2 content of the mélange protolith (Codillo et al., 2018). Furthermore, experimental studies indicate that Ti is highly insoluble in aqueous fluids; even highly saline fluids cannot liberate Ti from the slab (Rustioni et al., 2021) and hence do not have the capability to drastically alter the $\delta^{49/47}Ti$ of the mantle wedge. When an influx of aqueous fluids causes hydrous melting of mantle wedge peridotite, the Ti content of the peridotite protolith is too low to retain rutile in the residue (e.g., Grove et al., 2006; Till et al., 2012; Pirard and Hermann, 2015). As a result, $\delta^{49/47}Ti$ of hydrous partial melting of mantle wedge peridotite does not cause Ti isotope fractionation and the resultant melts are therefore expected to have the same $\delta^{49/47}Ti$ as N-MORB (Figure 5).

The oceanic crust and its sedimentary cover provide the only suitable protolith for partial melts in equilibrium with rutile. The Ti content of the protolith is sufficiently high (typically 1–2 wt.% TiO_2 in MORB and 0.5–1 wt.% TiO_2 in sediments), and hydrous partial melting at low temperature produces silicic partial melts in which the solubility of TiO_2 is low but still at least an order of magnitude higher than in fluids. Hence, rutile is retained in the residue up to at least 900 °C and our modelling (see section 4 and Figure 2) shows that partial melts of (altered) oceanic crust formed at 750–800 °C have fractionated $\delta^{49/47}Ti$ (0.24±0.06‰). Partial melts of the subducting slab are therefore the only plausible medium to impart the diagnostic $\delta^{49/47}Ti$ signature on arc magmas.

Moreover, slab melts in equilibrium with residual rutile can adequately explain the characteristic relative depletion in Nb and Ta of global arc magmas (e.g., Ryerson and Watson, 1987; Yogodzinski et al., 1995; Elliott et al., 1997; Turner and Langmuir, 2022a). Negative Nb anomalies by themselves, however, do not provide unambiguous evidence for slab melting. Slab-to-mantle wedge mass transfer by aqueous fluids can also impose a negative Nb anomaly on arc magmas due to the low solubility of Nb and Ta in fluids compared to other incompatible elements (Rustioni et al., 2021), but cannot impose elevated $\delta^{49/47}Ti$ on primitive arc lavas due to the lack of Ti mobility in such fluids. The difference between fluid- and partial melt-dominated mass transfer is clearly demonstrated by the samples in this study. All primitive arc lavas display clear relative depletions in Nb, but in several basaltic samples with $\delta^{49/47}Ti$ similar to N-MORB, including the majority of the Lesser Antilles samples (Figure 4), negative Nb anomalies are not associated with a fractionated Ti isotope signature (supplementary Figure S6). The lack of elevated $\delta^{49/47}Ti$ suggests fluid-dominated mass transfer in these Lesser Antilles samples, whereas the combination of relative Nb–Ta depletion and elevated $\delta^{49/47}Ti$ as seen in other primitive arc lavas in this study is uniquely attributable to slab melting.

Metabasite partial melts will have the same $^{143}Nd/^{144}Nd$ as their protolith (MORB; Figure 4b). Primitive Aleutian rhyodacites overlap with metabasite partial melts in Ti–Nd isotope space, in agreement with other geochemical data that suggest a strong slab melt signature in these samples (e.g., Yogodzinski et al., 1995; Yogodzinski et al., 2015; Yogodzinski et al., 2017). Samples from the other localities have lower $\delta^{49/47}Ti$, which suggests that they are not pure slab melts, but these lavas do require a variable contribution of a slab melt to explain their fractionated Ti isotope compositions. In general, Nd isotopes indicate that the slab melt

component recorded in the primitive arc lavas is predominantly derived from the (altered) oceanic crust with a subordinate contribution from the superjacent sedimentary veneer. Aegean arc lavas show the strongest metasediment melt signature, consistent with the thick subducted sediment package that is clearly expressed in the radiogenic isotope composition of Aegean arc lavas (e.g., Elburg et al., 2014; Klaver et al., 2016).

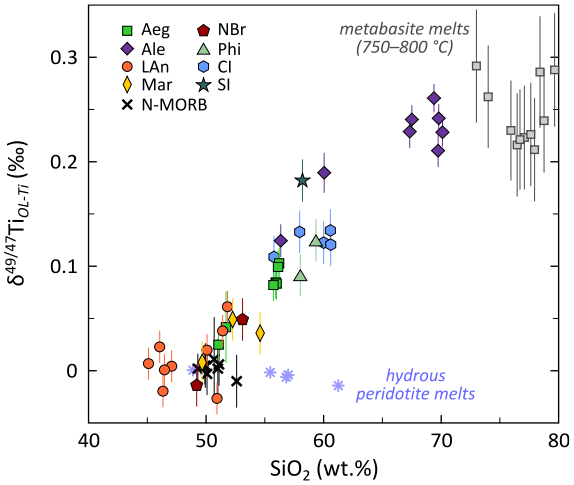

Figure 5. *Primitive arc lavas (Mg# ≥60) display a strong correlation between $\delta^{49/47}Ti$ and SiO_2 content. The composition of the metabasite partial melts at 750–800 °C (grey squares) is their $\Delta^{49/47}Ti_{melt-protolith}$ (Figure 2a) added to the average $\delta^{49/47}Ti$ of N-MORB (0.001‰; see Figure 1). The composition of hydrous peridotite melts is from experimental studies for peridotite+H_2O (Grove et al., 2006; Till et al., 2012) where $\delta^{49/47}Ti$ is calculated though an isotopic mass balance (as in Figure 2; see supplementary material for details), assuming that no Ti is transported to the mantle wedge by aqueous fluids (Rustioni et al., 2021) and mantle peridotite has $\delta^{49/47}Ti$ = 0. Sample location abbreviations: Aeg – Aegean arc; Ale – Aleutian arc; LAn – Lesser Antilles arc; Mar – Mariana arc; NBr – New Britain arc; Phi – Philippines arc; CI – Cook Island (Austral Volcanic Zone, Chile); SI – Solander Islands (New Zealand).*

5.4. How slab melts contribute to arc magmatism

Hydrous, silicic slab melts are in chemical disequilibrium with mantle wedge peridotite and will react to form orthopyroxene once released from the slab (e.g., Rapp et al., 1999; Pirard and Hermann, 2015). This reaction consumes some SiO_2 from the slab melt and leads to an increase in Mg# and compatible element contents (Cr, Ni) in the reacted melt while incompatible trace element patterns are preserved (e.g., Pirard and Hermann, 2015; Sisson and Kelemen, 2018; Lara and Dasgupta, 2020). Once formed, such orthopyroxene veins can act as pathways for subsequent batches of slab melt, leading to equilibration of melt Mg# with wall-rock orthopyroxene but otherwise leaving the major- and trace element signature of the slab melt unaffected (Rebaza et al., 2023).

The reaction that forms orthopyroxene veins will have little effect on the $\delta^{49/47}Ti$ of the percolating slab melt. Titanium is incompatible in orthopyroxene and hence the extraction of orthopyroxene from the melt will increase melt Ti content (Sisson and Kelemen, 2018). Equilibrium Ti isotope fractionation between silicate melt and orthopyroxene is negligible (Rzehak et al., 2021; see supplementary Figure S1). Hence, newly formed orthopyroxene is predicted to have a Ti isotope composition that mirrors that of the melt and does drive the melt to notably higher or lower $\delta^{49/47}Ti$. Even after substantive orthopyroxene formation $\delta^{49/47}Ti$ of the slab melt will be thus conserved.

The primitive rhyodacites from the Aleutian arc with $\delta^{49/47}Ti$ of 0.24±0.03‰ (Figures 4 and 5) are a rare example of such a process where silicic slab melts have traversed the mantle wedge with little modification besides Mg# equilibration and have erupted at the surface. This probably reflects the tectonic setting of western Aleutian rhyodacite volcanoes (Yogodzinski et al., 2015), which lie only 40–50 km above the top of the slab and just east of a physical opening in the subducting plate (Levin et al., 2005; Hayes et al., 2018). In this

setting significant melt production is expected because the temperature of the subducting oceanic crust must be well above the hydrous basalt solidus. The shallow depth means that, in turn, any melt that escapes the slab will have a relatively short pathway to the surface, thus limiting thermal and chemical exchange between the silicic melt and ambient mantle peridotite.

More commonly, however, ascending hydrous slab melts will trigger partial melting of the mantle wedge when the wet peridotite solidus is exceeded (Kelemen, 1995; Pirard and Hermann, 2015). Mixing with peridotite melts will attenuate the trace element and $\delta^{49/47}$Ti slab melt signature and produce a wide array of primary arc magma compositions that are blends of slab- and peridotite-derived melt. Nevertheless, elevated $\delta^{49/47}$Ti compared to N-MORB remains a uniquely sensitive tracer for the involvement of a slab melt even when this is diluted with peridotite melt in transit through the mantle wedge (Figure 4b).

Furthermore, the striking correlation between $\delta^{49/47}$Ti and SiO_2 content of primitive arc lavas (Figure 5) suggests that the elevated silica content of primitive (Mg# ≥60) andesites and (rhyo)dacites found worldwide (e.g., Kelemen et al., 2014) is a direct consequence of slab melting. We reiterate that although fluid-fluxed melting of mantle wedge peridotite can produce andesitic melts with high Mg# (e.g., Kushiro, 1972; Till et al., 2012), the lack of Ti mobility in fluids means that such partial melts do not have the elevated $\delta^{49/47}$Ti found in primitive andesites and (rhyo)dacites (Figure 5). Hence, Ti isotope systematics of primitive arc lavas provide strong support for slab melts as a key medium for mass transfer in subduction zones.

5.5. A recipe for widespread slab melting

The specific sensitivity of Ti isotopes to slab melting allows us to identify at least one sample with a slab melt component in all eight subduction zones for which $\delta^{49/47}$Ti compositions of primitive arc lavas are available (Figure 5). Primitive andesites and rhyodacites from the Aleutian arc, Cook Island, and Solander Islands have previously been interpreted in the light of a significant slab melt contribution (e.g., Kay, 1978; Yogodzinski et al., 1995; Stern and Kilian, 1996; Foley et al., 2014; Yogodzinski et al., 2017; see supplementary material), which is confirmed by the new Ti isotope data, but also arcs where primitive silicic magmas are rare show evidence for slab melting. For example, a reappraisal of previously published $\delta^{49/47}$Ti data for the New Britain arc and Mariana arc (Millet and Dauphas, 2014; Millet et al., 2016) leads us to recognize that one out of two New Britain, and two out of three Mariana primitive lavas show a combination of elevated SiO_2 content and $\delta^{49/47}$Ti (ca. 0.05‰) relative to N-MORB (Figure 5) that could be indicative of a modest but clearly resolvable slab melt contribution, though a more systematic study of Mariana and New Britain arc lavas is needed to substantiate this. Moreover, primitive basaltic andesites from the Aegean arc show clear Ti isotope evidence for an important role for slab melting ($\delta^{49/47}$Ti = ca. 0.10‰) whereas this had hitherto not been explicitly demonstrated. In the Lesser Antilles arc, there is no unambiguous Ti isotope evidence for slab melting in the southern islands (Grenada, St. Vincent, Bequia). The single sample from Saba, the northernmost active volcanic centre of the Lesser Antilles arc, does display elevated $\delta^{49/47}$Ti (0.06‰; Figure 4). The combined SiO_2–$\delta^{49/47}$Ti signature of this samples falls on the primitive arc lava array in Figure 5, consistent with a slab melt contribution, but lavas from Saba show evidence for magma mixing (Defant et al., 2001) and this process cannot be completely ruled out. In general, however, slab melting seems to be a widespread phenomenon in modern subduction zones.

The prevalence of slab melting in modern subduction zones raises the question of which conditions are required to allow melting of the subducted slab. Slab melting has often been related to the subduction of young and warm oceanic crust (e.g., Defant and Drummond, 1990). Recent dynamic models (Syracuse et al., 2010; van Keken et al., 2011; van Keken et al., 2018) and geochemical thermometry (Cooper et al., 2012), however, suggest that the temperature required for slab melting can be met in the majority of modern subduction zones. Based on the Ti isotope evidence for widespread slab melting, it appears that slab age is not the defining parameter that dictates whether the slab can melt. For example, the Aegean arc has the oldest (ca. 200 Ma) and therefore coldest subducting oceanic crust globally, yet lavas with a strong slab melt signature are erupted. Rather than slab age, the three-dimensional structure of the slab likely plays a pivotal role in providing additional sources of heat. In particular, tearing of the slab allows the inflow of

asthenospheric mantle that can heat the torn edge of the slab. This explanation has been invoked for the melting of the 50–60 Ma Pacific slab in the western Aleutian arc (Yogodzinski et al., 2001; Levin et al., 2005; Yogodzinski et al., 2017) and can also apply to the Aegean arc where lavas from Nisyros display Pb isotope evidence for toroidal mantle flow through a slab tear (Klaver et al., 2016).

Another prerequisite for slab melting is the presence of aqueous fluids to lower the solidus of the metabasite and metasediment. Insufficient water is probably present in the protolith at sub-arc depths to allow dehydration melting (e.g., Spandler and Pirard, 2013), and hence an external fluid source is required. Strontium isotope constraints suggest breakdown of serpentinite in the lithospheric mantle of the slab as an important source of aqueous fluids (Yogodzinski et al., 2017; Klaver et al., 2020). These fluids will travel up a temperature gradient in the slab and initiate hydrous partial melting when the wet solidus of metabasite and/or metasediment is crossed. In cold subduction zones where the temperature does not exceed the wet solidus of the slab, solute-rich aqueous fluids may still play an important role of slab-to-mantle wedge mass transfer (e.g., Keppler, 2017; Rustioni et al., 2021) and contribute to island arc basalt generation, but only slab melts can deliver fractionated Ti to the mantle wedge and produce silicic primitive arc magmas.

6. Conclusions

A comprehensive study of the Ti isotope composition of primitive arc lavas (Mg# ≥60) from eight global subduction zones indicates that primitive arc lavas display pronounced Ti isotope heterogeneity compared to basalts erupted at oceanic spreading centres (MORB) and within-plate settings. Normal MORB has homogeneous $\delta^{49/47}$Ti (0.001±0.015‰), consistent with an absence of Ti isotope fractionation during peridotite melting. In contrast, primitive arc lavas have strongly correlated $\delta^{49/47}$Ti and SiO_2 contents with the highest $\delta^{49/47}$Ti (0.24±0.03‰) recorded in primitive rhyodacites from the western Aleutian arc. The fractionated Ti isotope signature reflects melting in the presence of residual rutile, which can only plausibly take place in the subducted oceanic crust and its sedimentary cover. Hence, $\delta^{49/47}$Ti is a robust tracer of slab melting even when slab melts are diluted during interaction with the mantle wedge. The conclusions from this study can furthermore be summarised as follows:

- The modelled $\delta^{49/47}$Ti of hydrous metabasite partial melts at 750–800 °C and 2.6–4.5 GPa (0.24±0.06‰) matches that of primitive Aleutian rhyodacites (0.24±0.03‰), indicating that these Aleutian rhyodacites are slab melts that have traversed the mantle wedge with only little modification in the form of Mg# equilibration.
- The elevated $\delta^{49/47}$Ti of primitive andesites and rhyodacites rules out their generation through hydrous peridotite melting as the fractionated Ti signature cannot be carried to the mantle wedge by aqueous fluids and rutile is not stable in peridotite melting residua.
- In addition to the Aleutian arc, all other studied subduction zones also display evidence for slab melting, but in a more diluted form. Hydrous, silicic slab melts in transit through the mantle wedge promote additional peridotite melting, which dilutes the original slab melt signature and generates a wide spectrum of primary arc magmas that are blends of slab- and peridotite-derived melt.
- Slab melting therefore appears to be a common, widespread phenomenon in modern subduction zones, irrespective of slab age. Rather, three-dimensional effects such as the presence of slab tears can help raise the temperature of subducting slabs above their wet solidus. The influx of fluids released by serpentinite breakdown will then trigger hydrous melting of the oceanic crust and superjacent sediments.

Acknowledgements

This manuscript greatly benefitted from discussions with Pierre Bouilhol, Ben Maunder, Jeroen van Hunen, Tim Elliott, Julie Prytulak, Stephan Klemme, and Nikitha Saji. Jon Blundy and Richard Robertson are thanked for providing some of the Lesser Antilles samples; Felix Genske and Heidi Baier are thanked for their assistance with Sr–Nd isotope measurements made in Münster. Comments made by Steve Turner and an anonymous reviewer helped to improve this work. Rosemary Hickey-Vargas is thanked for editorial handling. This work was

supported by a Humboldt postdoctoral research fellowship to MK, NERC project NIIICE (NE/R001332/1) and a Royal Society Research Grant (RG150693) to MAM, as well as U.S. National Science Foundation grants to GY (OCE-1551640, EAR-1753518).

CRediT author statement

Martijn Klaver: Conceptualization, Formal Analysis, Investigation, Writing – Original Draft; **Gene Yogodzinski**: Conceptualization, Resources, Writing – Review & Editing, Funding Acquisition; **Capucine Albert**: Investigation; **Michal Camejo-Harry**: Resources; **Marlina Elburg**: Resources; **Kaj Hoernle**: Resources; **Colin Macpherson**: Resources, Writing – Review & Editing; **Geoff Nowell**: Resources; **Tracy Rushmer**: Resources, Writing – Review & Editing; **Helen Williams**: Resources, Writing – Review & Editing; **Marc-Alban Millet**: Conceptualization, Investigation, Writing – Review & Editing, Funding Acquisition.

REFERENCES

Aarons, S.M., Dauphas, N., Blanchard, M., Zeng, H., Nie, N.X., Johnson, A.C., Greber, N.D., Hopp, T., 2021. Clues from ab initio calculations on titanium isotopic fractionation in tholeiitic and calc-alkaline magma series. ACS earth and space chemistry 5, 2466-2480.

Alonso-Perez, R., Müntener, O., Ulmer, P., 2009. Igneous garnet and amphibole fractionation in the roots of island arcs: experimental constraints on andesitic liquids. Contrib. Mineral. Petrol. 157, 541-558.

Carter, L.B., Skora, S., Blundy, J., De Hoog, J., Elliott, T., 2015. An experimental study of trace element fluxes from subducted oceanic crust. J. Petrol. 56, 1585-1606.

Codillo, E., Le Roux, V., Marschall, H., 2018. Arc-like magmas generated by mélange-peridotite interaction in the mantle wedge. Nature communications 9, 1-11.

Coldwell, B., Adam, J., Rushmer, T., Macpherson, C., 2011. Evolution of the East Philippine Arc: experimental constraints on magmatic phase relations and adakitic melt formation. Contrib. Mineral. Petrol. 162, 835-848.

Cooper, L.B., Ruscitto, D.M., Plank, T., Wallace, P.J., Syracuse, E.M., Manning, C.E., 2012. Global variations in H2O/Ce: 1. Slab surface temperatures beneath volcanic arcs. Geochem. Geophys. Geosyst. 13.

Defant, M.J., Drummond, M.S., 1990. Derivation of some modern arc magmas by melting of young subducted lithosphere. Nature 347, 662-665.

Defant, M.J., Sherman, S., Maury, R.C., Bellon, H., De Boer, J., Davidson, J., Kepezhinskas, P., 2001. The geology, petrology, and petrogenesis of Saba Island, Lesser Antilles. J. Volcanol. Geotherm. Res. 107, 87-111.

Deng, Z., Chaussidon, M., Savage, P., Robert, F., Pik, R., Moynier, F., 2019. Titanium isotopes as a tracer for the plume or island arc affinity of felsic rocks. Proceedings of the National Academy of Sciences 116, 1132-1135.

Deng, Z., Moynier, F., Sossi, P., Chaussidon, M., 2018. Bridging the depleted MORB mantle and the continental crust using titanium isotopes. Geochemical Perspectives Letters 9, 11-15.

Deng, Z., Schiller, M., Jackson, M.G., Millet, M.-A., Pan, L., Nikolajsen, K., Saji, N.S., Huang, D., Bizzarro, M., 2023. Earth's evolving geodynamic regime recorded by titanium isotopes. Nature 621, 100-104.

Elburg, M.A., Smet, I., De Pelsmaeker, E., 2014. Influence of source materials and fractionating assemblage on magmatism along the Aegean Arc, and implications for crustal growth. Geological Society, London, Special Publications 385, 137-160.

Elliott, T., Plank, T., Zindler, A., White, W., Bourdon, B., 1997. Element transport from slab to volcanic front at the Mariana arc. Journal of Geophysical Research: Solid Earth 102, 14991-15019.

Foley, F.V., Turner, S., Rushmer, T., Caulfield, J.T., Daczko, N.R., Bierman, P., Robertson, M., Barrie, C.D., Boyce, A.J., 2014. ^{10}Be, ^{18}O and radiogenic isotopic constraints on the origin of adakitic signatures: a case study from Solander and Little Solander Islands, New Zealand. Contrib. Mineral. Petrol. 168, 1-28.

Gaetani, G.A., Asimow, P.D., Stolper, E.M., 2008. A model for rutile saturation in silicate melts with applications to eclogite partial melting in subduction zones and mantle plumes. Earth Planet. Sci. Lett. 272, 720-729.

Gill, J., 1981. Orogenic andesites and plate tectonics. Springer, Berlin.

Greber, N.D., Dauphas, N., Bekker, A., Ptáček, M.P., Bindeman, I.N., Hofmann, A., 2017. Titanium isotopic evidence for felsic crust and plate tectonics 3.5 billion years ago. Science 357, 1271-1274.

Greber, N.D., Pettke, T., Vilela, N., Lanari, P., Dauphas, N., 2021. Titanium isotopic compositions of bulk rocks and mineral separates from the Kos magmatic suite: Insights into fractional crystallization and magma mixing processes. Chem. Geol. 578, 120303.

Grove, T.L., Chatterjee, N., Parman, S.W., Médard, E., 2006. The influence of H_2O on mantle wedge melting. Earth Planet. Sci. Lett. 249, 74-89.

Hayes, G.P., Moore, G.L., Portner, D.E., Hearne, M., Flamme, H., Furtney, M., Smoczyk, G.M., 2018. Slab2, a comprehensive subduction zone geometry model. Science 362, 58-61.

Hermann, J., Spandler, C., Hack, A., Korsakov, A.V., 2006. Aqueous fluids and hydrous melts in high-pressure and ultra-high pressure rocks: Implications for element transfer in subduction zones. Lithos 92, 399-417.

Hernández-Uribe, D., Hernández-Montenegro, J.D., Cone, K.A., Palin, R.M., 2020. Oceanic slab-top melting during subduction: Implications for trace-element recycling and adakite petrogenesis. Geology 48, 216-220.

Hoare, L., Klaver, M., Muir, D.D., Klemme, S., Barling, J., Parkinson, I.J., Lissenberg, C.J., Millet, M.-A., 2022. Empirical and experimental constraints on Fe-Ti oxide-melt titanium isotope fractionation factors. Geochim. Cosmochim. Acta 326, 253-272.

Hoare, L., Klaver, M., Saji, N.S., Gillies, J., Parkinson, I.J., Lissenberg, C.J., Millet, M.-A., 2020. Melt chemistry and redox conditions control titanium isotope fractionation during magmatic differentiation. Geochim. Cosmochim. Acta 282, 38-54.

Johnson, M.C., Plank, T., 1999. Dehydration and melting experiments constrain the fate of subducted sediments. Geochem. Geophys. Geosyst. 1.

Kay, R.W., 1978. Aleutian magnesian andesites: melts from subducted Pacific Ocean crust. J. Volcanol. Geotherm. Res. 4, 117-132.

Kelemen, P.B., 1995. Genesis of high Mg# andesites and the continental crust. Contrib. Mineral. Petrol. 120, 1-19.

Kelemen, P.B., Hanghøj, K., Greene, A.R., 2014. One view of the geochemistry of subduction-related magmatic arcs, with an emphasis on primitive andesite and lower crust, in: Holland, H.D., Turekian, K.K. (Eds.), Treatise on geochemistry (2nd edition). Elsevier, Oxford, pp. 749-805.

Keppler, H., 2017. Fluids and trace element transport in subduction zones. Am. Mineral. 102, 5-20.

Kessel, R., Schmidt, M.W., Ulmer, P., Pettke, T., 2005a. Trace element signature of subduction-zone fluids, melts and supercritical liquids at 120–180 km depth. Nature 437, 724-727.

Kessel, R., Ulmer, P., Pettke, T., Schmidt, M., Thompson, A., 2005b. The water–basalt system at 4 to 6 GPa: Phase relations and second critical endpoint in a K-free eclogite at 700 to 1400 C. Earth Planet. Sci. Lett. 237, 873-892.

Klaver, M., Davies, G.R., Vroon, P.Z., 2016. Subslab mantle of African provenance infiltrating the Aegean mantle wedge. Geology 44, 367-370.

Klaver, M., Lewis, J., Parkinson, I.J., Elburg, M.A., Vroon, P.Z., Kelley, K.A., Elliott, T., 2020. Sr isotopes in arcs revisited: tracking slab dehydration using $\delta^{88/86}Sr$ and $^{87}Sr/^{86}Sr$ systematics of arc lavas. Geochim. Cosmochim. Acta 288, 101-119.

Klaver, M., MacLennan, S.A., Ibañez-Mejia, M., Tissot, F.L.H., Vroon, P.Z., Millet, M.-A., 2021. Reliability of detrital marine sediments as proxy for continental crust composition: The effects of hydrodynamic sorting on Ti and Zr isotope systematics. Geochim. Cosmochim. Acta 310, 221-239.

Kommescher, S., Kurzweil, F., Fonseca, R.O.C., Rzehak, L.J.A., Hohl, S.V., Kirchenbaur, M., Schuth, S., Sprung, P., Münker, C., 2023. Mineralogical Controls on the Ti Isotope Composition of Subduction Zone Magmas. Geochem. Geophys. Geosyst. 24, e2022GC010840.

Kushiro, I., 1972. Effect of water on the composition of magmas formed at high pressures. J. Petrol. 13, 311-334.

Lara, M., Dasgupta, R., 2020. Partial melting of a depleted peridotite metasomatized by a MORB-derived hydrous silicate melt–Implications for subduction zone magmatism. Geochim. Cosmochim. Acta 290, 137-161.

Levin, V., Shapiro, N.M., Park, J., Ritzwoller, M.H., 2005. Slab portal beneath the western Aleutians. Geology 33, 253-256.

Li, H., Hermann, J., Zhang, L., 2022. Melting of subducted slab dictates trace element recycling in global arcs. Science Advances 8, eabh2166.

Macpherson, C.G., Dreher, S.T., Thirlwall, M.F., 2006. Adakites without slab melting: high pressure differentiation of island arc magma, Mindanao, the Philippines. Earth Planet. Sci. Lett. 243, 581-593.

Mann, U., Schmidt, M.W., 2015. Melting of pelitic sediments at subarc depths: 1. Flux vs. fluid-absent melting and a parameterization of melt productivity. Chem. Geol. 404, 150-167.
Martin, L.A., Hermann, J., 2018. Experimental phase relations in altered oceanic crust: implications for carbon recycling at subduction zones. J. Petrol. 59, 299-320.
Martindale, M., Skora, S., Pickles, J., Elliott, T., Blundy, J., Avanzinelli, R., 2013. High pressure phase relations of subducted volcaniclastic sediments from the west pacific and their implications for the geochemistry of Mariana arc magmas. Chem. Geol. 342, 94-109.
Millet, M.-A., Dauphas, N., 2014. Ultra-precise titanium stable isotope measurements by double-spike high resolution MC-ICP-MS. J. Anal. At. Spectrom. 29, 1444-1458.
Millet, M.-A., Dauphas, N., Greber, N.D., Burton, K.W., Dale, C.W., Debret, B., Macpherson, C.G., Nowell, G.M., Williams, H.M., 2016. Titanium stable isotope investigation of magmatic processes on the Earth and Moon. Earth Planet. Sci. Lett. 449, 197-205.
Nielsen, S.G., Marschall, H.R., 2017. Geochemical evidence for mélange melting in global arcs. Science Advances 3, e1602402.
Pirard, C., Hermann, J., 2015. Focused fluid transfer through the mantle above subduction zones. Geology 43, 915-918.
Plank, T., Langmuir, C.H., 1993. Tracing trace elements from sediment input to volcanic output at subduction zones. Nature 362, 739-743.
Plank, T., Langmuir, C.H., 1998. The chemical composition of subducting sediment and its consequences for the crust and mantle. Chem. Geol. 145, 325-394.
Rapp, R., Shimizu, N., Norman, M., Applegate, G., 1999. Reaction between slab-derived melts and peridotite in the mantle wedge: experimental constraints at 3.8 GPa. Chem. Geol. 160, 335-356.
Rebaza, A.M., Mallik, A., Straub, S.M., 2023. Multiple episodes of rock-melt reaction at the slab-mantle interface: Formation of high silica primary magmas in intermediate to hot subduction zones. J. Petrol. 64, 1-20.
Rustioni, G., Audetat, A., Keppler, H., 2021. The composition of subduction zone fluids and the origin of the trace element enrichment in arc magmas. Contrib. Mineral. Petrol. 176, 51.
Ryerson, F.J., Watson, E.B., 1987. Rutile saturation in magmas: implications for Ti-Nb-Ta depletion in island-arc basalts. Earth Planet. Sci. Lett. 86, 225-239.
Rzehak, L.J., Kommescher, S., Kurzweil, F., Sprung, P., Leitzke, F.P., Fonseca, R.O., 2021. The redox dependence of titanium isotope fractionation in synthetic Ti-rich lunar melts. Contrib. Mineral. Petrol. 176, 1-16.
Rzehak, L.J.A., Kommescher, S., Hoare, L., Kurzweil, F., Sprung, P., Leitzke, F.P., Fonseca, R.O.C., 2022. Redox-dependent Ti stable isotope fractionation on the Moon: implications for current lunar magma ocean models. Contrib. Mineral. Petrol. 177, 1-20.
Schmidt, M.W., Vielzeuf, D., Auzanneau, E., 2004. Melting and dissolution of subducting crust at high pressures: the key role of white mica. Earth Planet. Sci. Lett. 228, 65-84.
Sisson, T., Kelemen, P., 2018. Near-solidus melts of MORB + 4 wt% H_2O at 0.8–2.8 GPa applied to issues of subduction magmatism and continent formation. Contrib. Mineral. Petrol. 173, 1-23.
Skora, S., Blundy, J., 2010. High-pressure hydrous phase relations of radiolarian clay and implications for the involvement of subducted sediment in arc magmatism. J. Petrol. 51, 2211-2243.
Skora, S., Blundy, J.D., Brooker, R.A., Green, E.C., de Hoog, J., Connolly, J.A., 2015. Hydrous phase relations and trace element partitioning behaviour in calcareous sediments at subduction-zone conditions. J. Petrol. 56, 953-980.
Spandler, C., Pirard, C., 2013. Element recycling from subducting slabs to arc crust: a review. Lithos 170, 208-223.
Stern, C.R., Kilian, R., 1996. Role of the subducted slab, mantle wedge and continental crust in the generation of adakites from the Andean Austral Volcanic Zone. Contrib. Mineral. Petrol. 123, 263-281.
Syracuse, E.M., van Keken, P.E., Abers, G.A., 2010. The global range of subduction zone thermal models. Phys. Earth Planet. Inter. 183, 73-90.
Tatsumi, Y., 1989. Migration of fluid phases and genesis of basalt magmas in subduction zones. Journal of Geophysical Research: Solid Earth 94, 4697-4707.
Tera, F., Brown, L., Morris, J., Sacks, I.S., Klein, J., Middleton, R., 1986. Sediment incorporation in island-arc magmas: Inferences from ^{10}Be. Geochim. Cosmochim. Acta 50, 535-550.
Till, C.B., Grove, T.L., Withers, A.C., 2012. The beginnings of hydrous mantle wedge melting. Contrib. Mineral. Petrol. 163, 669-688.
Turner, S.J., Langmuir, C.H., 2022a. A quantitative framework for global variations in arc geochemistry. Earth Planet. Sci. Lett. 584, 117411.

Turner, S.J., Langmuir, C.H., 2022b. Sediment and ocean crust both melt at subduction zones. Earth Planet. Sci. Lett. 584, 117424.
van Keken, P.E., Hacker, B.R., Syracuse, E.M., Abers, G.A., 2011. Subduction factory: 4. Depth-dependent flux of H2O from subducting slabs worldwide. Journal of Geophysical Research: Solid Earth 116.
van Keken, P.E., Wada, I., Abers, G.A., Hacker, B.R., Wang, K., 2018. Mafic high-pressure rocks are preferentially exhumed from warm subduction settings. Geochem. Geophys. Geosyst. 19, 2934-2961.
White, W.M., Dupré, B., 1986. Sediment subduction and magma genesis in the Lesser Antilles: isotopic and trace element constraints. Journal of Geophysical Research: Solid Earth (1978–2012) 91, 5927-5941.
Xiong, X., Keppler, H., Audétat, A., Gudfinnsson, G., Sun, W., Song, M., Xiao, W., Yuan, L., 2009. Experimental constraints on rutile saturation during partial melting of metabasalt at the amphibolite to eclogite transition, with applications to TTG genesis. Am. Mineral. 94, 1175-1186.
Yogodzinski, G., Kay, R., Volynets, O., Koloskov, A., Kay, S., 1995. Magnesian andesite in the western Aleutian Komandorsky region: implications for slab melting and processes in the mantle wedge. Geol. Soc. Am. Bull. 107, 505-519.
Yogodzinski, G., Lees, J., Churikova, T., Dorendorf, F., Wöerner, G., Volynets, O., 2001. Geochemical evidence for the melting of subducting oceanic lithosphere at plate edges. Nature 409, 500-504.
Yogodzinski, G.M., Brown, S.T., Kelemen, P.B., Vervoort, J.D., Portnyagin, M., Sims, K.W., Hoernle, K., Jicha, B.R., Werner, R., 2015. The role of subducted basalt in the source of island arc magmas: evidence from seafloor lavas of the western Aleutians. J. Petrol. 56, 441-492.
Yogodzinski, G.M., Kelemen, P.B., Hoernle, K., Brown, S.T., Bindeman, I., Vervoort, J.D., Sims, K.W., Portnyagin, M., Werner, R., 2017. Sr and O isotopes in western Aleutian seafloor lavas: Implications for the source of fluids and trace element character of arc volcanic rocks. Earth Planet. Sci. Lett. 475, 169-180.

SUPPLEMENTARY MATERIAL

Supplementary Datasets

Microsoft Excel files available at: https://doi.org/10.1016/j.epsl.2023.118544

Dataset 1 Titanium isotope partial melting models for metabasite, metasediment, and peridotite.

Dataset 2 Titanium isotope composition data for samples measured in this study, reference materials measures alongside the samples at Cardiff University, trace element and Sr–Nd isotope data for the Lesser Antilles samples, and full geochemical characterisation of the samples measured in this study as well as literature data for N-MORB and subducting sediments.

1. Modelling Ti isotope fractionation during partial melting

Mass-dependent isotope fractionation during partial melting results from differences in bonding environment of an element between the partial melt and the solid phases in the melting residue (e.g., Young et al., 2015). Isotopic fractionation factors between phases (denoted as α_{i-j} for phases *i* and *j*, where a phase can be a mineral, melt, metal, etc.) dictate the sign and magnitude of isotopic fractionation. Recently, quantitative constraints on the magnitude of Ti isotope fractionation between minerals and melt have become available through measurement of natural or experimental mineral–melt pairs and *ab initio* simulations based on density functional theory. These quantitative constraints allow forward modelling of Ti isotope fractionation during hydrous partial melting of metabasite and metasediment.

The key parameter for our melting models is the rutile–melt Ti isotope fractionation factor. We employ the weighted mean of rutile–melt Ti isotope fractionation factors determined from three experimental rutile–melt pairs reported in two recent studies (Hoare et al., 2022; Rzehak et al., 2022) as given in Table S1. In addition, there are independent constraints on the mineral–melt Ti isotope fractionation factors for titanomagnetite

(Hoare et al., 2022) and orthopyroxene with Ti^{4+} in VI-fold coordination (Rzehak et al., 2021), which are also listed in Table S1 and shown in Figure S1. For other minerals relevant for this study, no direct data for mineral–melt Ti isotope fractionation are available, but these can be derived from *ab initio* simulations that report reduced partition function ratios (RPFR, β_i) for Ti in various minerals (Leitzke et al., 2018; Wang et al., 2020; Aarons et al., 2021; Table S2). As the fractionation factor between two phases is the ratio of the RPFRs of these phases ($\alpha_{i-j} = \beta_i/\beta_j$), *ab initio* constraints allow calculation of mineral–melt Ti isotope fractionation factor relative to the anchor of the $\alpha_{rutile-melt}$ (Table S1):

$$\alpha_{i-melt} = \frac{\beta_i}{\beta_{rt}} * \alpha_{rt-melt}$$

We use *ab initio* constraints on the RPFR of rutile, olivine (Ti in IV-fold coordination), and garnet (pyrope, Ti in VI-fold coordination) from Wang et al. (2020) and clinopyroxene with Ti^{4+} substitution for Mg in the octahedral site (VI-fold coordination) from Leitzke et al. (2018), as summarised in Table S2. For several other minerals, notably phengite, neither direct mineral–melt Ti isotope fractionation factors nor *ab initio* RPFRs are available. In phengite and biotite, which can hold a considerable fraction of Ti in the melting residue of metasediments, Ti occurs in the octahedral site in VI-fold coordination (e.g., Auzanneau et al., 2010) and we therefore estimate their RPFRs to be identical to that of garnet (Table S2). This is supported by data for mineral separates that suggest that biotite is isotopically heavier than Fe-Ti oxides and has $\delta^{49/47}$Ti similar to other silicate minerals (Greber et al., 2021; Nie et al., 2021). Spinel *sensu stricto* has a similar structure to titanomagnetite, which is also a spinel-group mineral (O'Neill and Navrotsky, 1983). Hoare et al. (2022) found that the Ti isotope fractionation factor for titanomagnetite depends on its Ti content (Table S1), which was subsequently corroborated by Johnson et al. (2023). Following Hoare et al. (2022), we extrapolate this relationship to Ti-poor spinel yielding a spinel–melt Ti isotope fractionation factor close to unity (Figure S1). Epidote (Ti in VI-fold coordination, similar to garnet) and kyanite (Ti in IV-fold coordination, similar to olivine) are insignificant Ti sinks and the estimate of their fractionation factors has negligible influence on the modelling results.

Experimental studies and melting models (e.g., pMELTS) give the phase proportions, Ti concentration of the melt and residual phases, and the melting temperature. The latter is important as it determines the magnitude of isotopic fractionation factors as these are inversely proportional to square of the absolute temperature (Tables S1 and S2). With the mineral–melt fractionation factors in hand, a simple mass balance calculation can be employed to determine the Ti isotope composition of the partial melt relative to the protolith as follows (see e.g., Klaver et al., 2021a for a derivation):

$$\Delta^{49/47}Ti_{melt-protolith} = \frac{\sum_i (C_i F_i)}{\sum_i (C_i F_i \alpha_i)} - 1$$

Where C_i is the Ti concentration in phase *i*, F_i is weight fraction of phase *i*, and α_i is the mineral–melt Ti isotope fractionation factor for phase *i*. Note that the melt has to be included as a phase with $\alpha_{melt} = 1$. The uncertainty on the rutile–melt Ti isotope fractionation factor (Table S1) was taken as the sole source of uncertainty in the melting models as it is not possible to determine the uncertainty on *ab initio* simulations and RPFRs. The rutile–melt uncertainty is propagated through the melting model using standard linear uncertainty propagation. In rare cases where both titanomagnetite and rutile were present in the melting residue, we propagated the uncertainty on both fractionation factors (Table S1) with the aid of a Monte Carlo simulation.

Table S1. Titanium mineral–melt fractionation factors

phase	fractionation factor*	reference
rutile	$10^3\ln\alpha_{rt-melt} = -0.444\pm0.028 \times 10^6/T^2$	Hoare et al. (2022), Rzehak et al. (2022)
titanomagnetite *(and spinel)*	$10^3\ln\alpha_{Ti\text{-}mag-melt} = [-0.0482\pm0.0069 \times TiO_{2(Ti\text{-}mag)} + 0.0530\pm0.1203] \times 10^6/T^2$	Hoare et al. (2022)
orthopyroxene $^{[VI]}Ti^{4+}$	$10^3\ln\alpha_{opx-melt} = -0.008 \times 10^6/T^2$	Rzehak et al. (2021)

**temperature (T) in K*

Table S2. Titanium reduced partition function ratios ($10^3\ln\beta$)*

phase	formula	a	b	c	reference
rutile	Ti_2O_4	1.19767	-0.00959	0.000154	Wang et al. (2020)
olivine $^{[IV]}Ti^{4+}$	$Mg_{64}Si_{31}TiO_{128}$	2.33041	-0.04105	0.001092	Wang et al. (2020)
clinopyroxene $^{[VI]}Ti^{4+}$		1.69903	-0.00972	0.000127	Leitzke et al. (2018)
garnet (pyrope) $^{[VI]}Ti^{4+}$	$Mg_{12}Al_7TiSi_{11}AlO_{48}$	1.70195	-0.01864	0.000380	Wang et al. (2020)
phengite, biotite $^{[VI]}Ti^{4+}$			*same as garnet*		
epidote $^{[VI]}Ti^{4+}$			*same as garnet*		
kyanite $^{[IV]}Ti^{4+}$			*same as olivine*		

**$10^3 ln\beta = ax + bx^2 + cx^3$ where $x = 10^6/T^2$ (T in K)*

We test the validity of the Ti isotope fractionation factors employed here with a pMELTS (Ghiorso et al., 2002) batch melting model of an anhydrous primitive mantle (Palme and O'Neill, 2014) peridotite composition at 1 and 2.5 GPa. Partial melts (2–30% melt) of such a primitive mantle composition display negligible Ti isotope fractionation relative to the bulk protolith ($\Delta^{49/47}Ti_{melt-protolith}$ = -0.023 – +0.006‰; see Figure 2 in the main text). The absence of pronounced Ti isotope fractionation during mantle melting (without rutile as a residual phase) is consistent with the overlap in $\delta^{49/47}Ti$ between chondrites (Greber et al., 2017b; Williams et al., 2021), peridotites (Millet et al., 2016; Anguelova et al., 2022), and mafic to ultramafic volcanic rocks (Millet et al., 2016; Greber et al., 2017b; Deng et al., 2018; Hoare et al., 2020; Zhao et al., 2020).

Modelling of Ti isotope fractionation during hydrous partial melting of (altered) basalt and various sediment lithologies is based is based on experimental studies that are summarised in Table S3. The Ti mass balance between partial melt and residual minerals is based on reported Ti concentration data and phase proportions calculated through least squares mass balance on an anhydrous basis (see supplementary Dataset 1). Subsequently, we employed the isotopic mass balance discussed above to calculate $\Delta^{49/47}Ti_{melt-protolith}$ for the experimental runs at different temperatures and pressures (Figure 2 in the main text). The presence of rutile dictates that most Ti is retained in the melting residua. Given the strong preference of rutile for the lighter isotopes of Ti, the partial melts have clearly elevated $\Delta^{49/47}Ti_{melt-protolith}$, but the Ti isotope composition of the melting residua is barely affected (Figure S2). See main text for a more detailed discussion of the melting models.

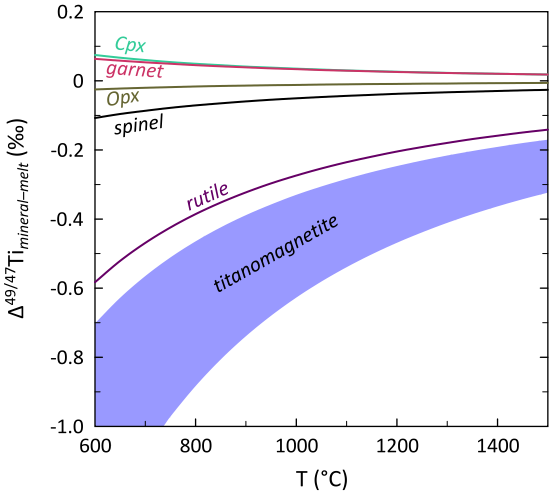

Figure S1. *Average mineral–melt Ti isotope fractionation factors used in this study as tabulated in Tables S1 and S2. Titanomagnetite is shown as a shaded field for titanomagnetite TiO_2 content between 10 and 20 wt.%; spinel is calculated using the relationship for titanomagnetite containing 0.5 wt.% TiO_2, as appropriate for spinel in fertile lherzolites. A lower spinel TiO_2 content will bring the fractionation factor even closer to zero.*

Table S3. Overview of experimental studies used for Ti isotope melting models

reference	composition	TiO_2 (wt.%)	K_2O (wt.%)	H_2O (wt.%)	P (GPa)
basalts					
Schmidt et al. (2004)	K-rich MORB	2.0	0.9	1.8	4
Kessel et al. (2005)	MORB	1.49	0	13–18	4
Carter et al. (2015)	altered MORB	1.58	0.25	15	3
Sisson and Kelemen (2018)	MORB	1.91	0.19	4	2.6–2.8
Martin and Hermann (2018)	altered MORB	1.23	0.98	7.5	3–4.5
sediments					
Mann and Schmidt (2015)	pelite	0.84	2.4	1.5–4.4	3
Skora and Blundy (2010)	radiolarian clay	0.87	2.02	7–15	3
Skora et al. (2015)	calcareous	0.93	2.53	8–23	3
Martindale et al. (2013)	volcaniclastic	1.85	2.61	ca. 20	3–6

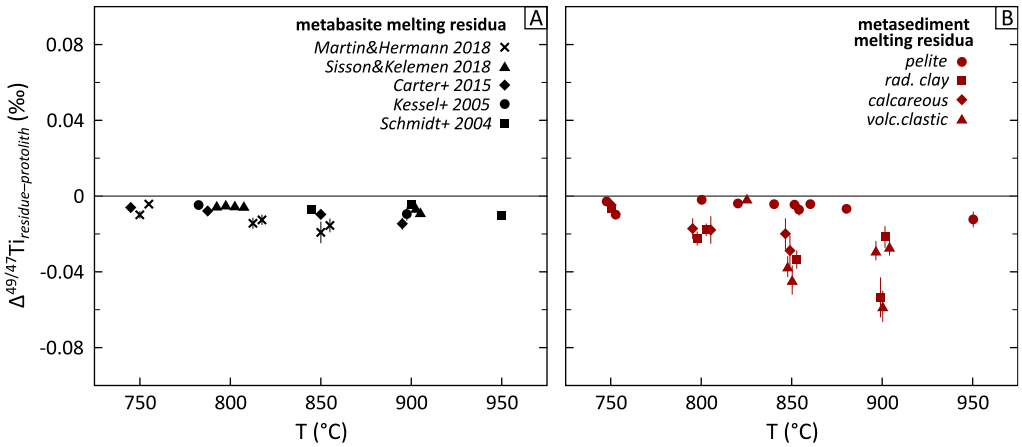

Figure S2. *Modelled Ti isotope fractionation between the residue and protolith during hydrous melting of (altered) MORB (A) and various sediment lithologies (B) at 2.6–6 GPa based on experimental studies (Schmidt et al., 2004; Kessel et al., 2005; Skora and Blundy, 2010; Martindale et al., 2013; Carter et al., 2015; Mann and*

Schmidt, 2015; Skora et al., 2015; Martin and Hermann, 2018; Sisson and Kelemen, 2018). The Ti isotope fractionation of the partial melt relative to the protolith ($\Delta^{49/47}Ti_{melt-protolith}$) can be calculated using Ti isotope mineral–melt fractionation factors (supplementary Tables S1 and 2) and is shown in Figure 2 in the main text. This figures shows the composition of the complimentary melting residua.

2. Additional analytical techniques

Titanium isotope ratio measurements

For the samples measured for Ti isotope composition at Cardiff University (Aegean arc, Aleutian arc, and Lesser Antilles arc samples), two to four repeat measurements were made to improve the measurement precision. Geological (BHVO-2, JB-2) and Ti solution (Alfa Aesar Ti wire and Alfa Aesar Ti solution) reference materials measured alongside the arc samples yield a pooled $2\overline{s}$ intermediate precision of 0.030‰ on $\delta^{49/47}$Ti (n = 33; Figure S3), which is similar to the pooled $2\overline{s}$ measurement precision of the repeat sample measurements (0.026‰). We take the intermediate precision of the reference material measurements ($2\overline{s}$ = 0.030‰) as the best estimate of the uncertainty on individual sample measurements, where the uncertainty on the average of the *n* repeat sample measurements is given by $2s_n = 2\overline{s}/\sqrt{n}$.

The arc lava samples measured at Durham University (Philippines arc, Solander Islands, Cook Island) were included in the same batches as samples reported by Millet et al. (2016). Hence, the reference material measurements listed in that study also reflect the uncertainty on the Durham arc lava measurements. Millet et al. (2016) report a 2s intermediate precision of 0.020‰ on $\delta^{49/47}$Ti (see Figure 1 in Millet et al., 2016), which is slightly better than for the Cardiff sample measurements. The exact same Ti purification procedure, double spike, and OL-Ti reference material were used in both labs, and the only difference is the MC-ICP-MS instrument used. In this case, it therefore seems that the Neptune at Durham University slightly outperformed the Nu Plasma II at Cardiff University. A potential factor contributing to this is the on average higher sensitivity (ion beam intensity per analyte concentration) of the Neptune due to its higher extraction voltage. The slightly poorer intermediate precision achieved in Cardiff is mitigated by making several repeat measurements per sample, as described above. Importantly, there is no bias between the two laboratories; average $\delta^{49/47}$Ti for reference materials agree very well between Durham and Cardiff (BHVO-2: 0.020±0.023‰ *versus* 0.030±0.019‰; JB-2: -0.046±0.017‰ *versus* -0.022±0.041‰, respectively), and with results published by other groups (open circles in Figure S3).

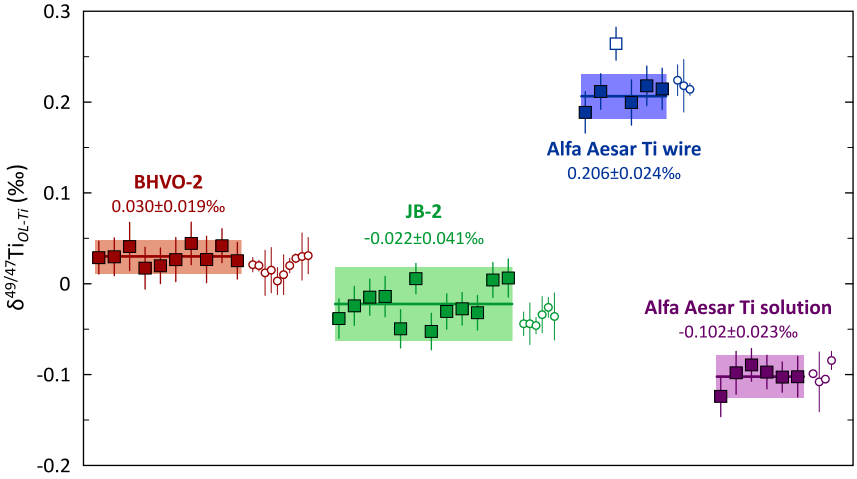

Figure S3. *Results for reference materials measured at Cardiff University alongside the samples in this study. One measurement of Alfa Aesar Ti wire is excluded as outlier based on Chauvenet's criterion (open square) and not included in the average. The pooled $2\overline{s}$ intermediate precision of these four reference materials is 0.030‰. Small open circles are literature data (Millet and Dauphas, 2014; Millet et al., 2016; Greber et al., 2017a; Greber et al., 2017b; Deng et al., 2018; Deng et al., 2019; Johnson et al., 2019; Aarons et al., 2020; Hoare et al., 2020;*

Kommescher et al., 2020; Klaver et al., 2021b; Williams et al., 2021; Hoare et al., 2022). See Figure 1 in Millet et al. (2016) for a similar figure for reference material measurements made alongside the samples measured in Durham.

Lesser Antilles trace element and Sr–Nd measurements

Trace element and radiogenic Sr–Nd isotope characterization of the Lesser Antilles samples, except for Grenada sample AMG 6103 from Thirlwall et al. (1996), was carried out at the WWU Münster (Germany); results are provided in supplementary Dataset 2. An aliquot of ca. 80–100 mg sample powder was digested in concentrated HF–HNO_3 and subsequently treated repeatedly with concentrated HCl and HNO_3 to eliminate fluorides. Subsequently, a ca. 5000 times gravimetric dilution was made of the sample solutions (i.e., 1 mg original sample material dissolved in 5 g 1 M HNO_3) for trace element measurements using an Element-2 sector field ICP-MS. The Element was tuned for sensitivity while keeping oxide production low (U/UO ≤ 0.03%). The samples were measured against a calibration curve consisting of gravimetric dilutions of geological reference materials BHVO-2, JB-2, and AGV-2. A separate solution of BHVO-2 measured as unknown indicates overall better than 5% agreement between measured and recommended values for this reference material.

Strontium was separated from the matrix using a conventional method with Sr spec resin. Neodymium was isolated using a two-step method consisting of REE separation using cationic AG50w-X8 resin followed by Nd purification with Ln resin in 0.2 M HCl. Isotope composition measurements were made using a Neptune MC-ICP-MS instrument with an ApexΩ desolvating nebuliser operated in low resolution mode. Strontium isotope data were corrected for Rb and Kr interference followed by exponential law internal normalization to $^{86}Sr/^{88}Sr$ = 0.1194. Repeat measurements of NIST SRM 987 ($^{87}Sr/^{86}Sr$ = 0.710203±0.000020; 2s, *n* = 8) show a small bias relative to the preferred value (0.710248; Thirlwall, 1991) and hence a linear correction of +0.000045 was made to all sample measurements. Corrected data for geological reference materials BHVO-2 (0.703478) and AGV-2 (0.703992) are in excellent agreement with recommended values. For Nd isotope composition measurements, the Neptune was tuned for low oxide production ($^{145}Nd^{16}O/^{145}Nd$ <0.01). Raw data were corrected for isobaric interference of Sm followed by exponential law internal normalization to $^{146}Nd/^{144}Nd$ = 0.721903. Repeat measurements of the JNdi reference material yield $^{143}Nd/^{144}Nd$ = 0.512095±0.000008 (2s, *n* = 8) and also geological reference materials BHVO-2 (0.512970) and AGV-2 (0.512773) yield results in excellent agreement with recommended values.

3. Primitive arc lava samples

Table S4. Overview of sample localities

sample suite	#samples* all (publ.)	#samples Mg# ≥60	dip angle (°)	subducting crust age (Ma)	upper crust type†
Aegean arc	18 (8)	7	30	ca. 200	TC
Aleutian arc	8	8	56	56	O
Lesser Antilles arc	10	9	42–50	90–120	O
Kermadec arc	7 (7)	-	56	106	O
Mariana arc	3 (3)	3	57	152	O
New Britain arc	8 (8)	2	68	25	O
Philippines arc	11	2	64	60	TC
Cook Island (Austral Volcanic Zone, Chile)	5	5	-	25	TC
Solander Islands (New Zealand)	8	1	-	20–50	TC

*Full data for all samples considered in this study are given in supplementary Dataset 2. Subduction zone dip angle and subducting crust age from Syracuse et al. (2010) and references in main text below. *number of samples, of which previously published in brackets. †TC – thin continental crust (<30 km); O – oceanic.*

Aegean arc

The present-day Aegean arc (Greece) is the volcanic expression of the terminal stage of subduction of oceanic lithosphere of the Tethys ocean that started in the Jurassic (van Hinsbergen et al., 2005). The exact age of the subducting oceanic lithosphere is unknown but it is estimated at 200 Ma, making it stand out as the oldest subducting crust globally (Syracuse et al., 2010). Quaternary volcanoes in the central–eastern section of the arc (Santorini, Nisyros) are built on thinned continental crust under an extensional stress regime (Tirel et al., 2004). As a result, magma mixing is a relatively uncommon process in these two volcanoes, and selected samples from Santorini represent a unique calk-alkaline differentiation suite linked through fractional crystallisation of an amphibole-free mineral assemblage (Druitt et al., 1999; Hoare et al., 2020; see Figure 3a in the main text). Primitive samples from Santorini and Nisyros show notable geochemical differences that have been attributed to upwelling of sub-slab asthenospheric mantle through a slab tear below western Anatolia (Klaver et al., 2016). In contrast with Santorini, basaltic lavas are absent from Nisyros; primitive samples (Mg# ≥60) are basaltic andesites with 54–58 wt.% SiO_2 that do not display petrographic evidence for mixing between mafic and felsic melts (e.g., Vanderkluysen et al., 2005; Elburg et al., 2014; Klaver et al., 2017; Klaver et al., 2018). Primitive Nisyros samples are characterised by high Sr contents (up to 1070 µg/g; Figure S4), high Sr/Nd and Sr/Y (both up to 70), and a decoupling of Sr and Nd isotopes (unradiogenic Nd isotope compositions indicative of a large subducted sediment input, but relatively low $^{87}Sr/^{86}Sr$ and MORB-like $\delta^{88/86}Sr$), which was interpreted as resulting from a large fluid contribution from serpentinite breakdown that triggered wet partial melting of the altered oceanic crust and thick sediment cover of the slab (Klaver et al., 2020).

Aleutian arc

The Aleutian arc is famous for the common occurrence of andesites, dacites, and rhyodacites with high Mg# and fractionated trace element patterns (e.g., high Sr/Y and La/Yb) that are interpreted as slab melts (e.g., Kay, 1978; Yogodzinski et al., 1995; Kelemen et al., 2003). We have selected several end-member primitive silica-rich lavas from the Aleutian arc for Ti isotope composition measurements. These samples include Miocene-age primitive andesites from Adak Island (56.4 wt.% SiO_2) and a dredge sample from the Komandorsky Straits near Kamchatka (60.1 wt.% SiO_2). In addition, we include six of the most Si-rich primitive arc lavas found globally: seafloor Pleistocene–Holocene primitive rhyodacites (67–70 wt.% SiO_2) collected from Western Cones area, west of the westernmost emergent volcano (Buldir) in the western Aleutian arc, by dredging from the R.V. *Sonne* (cruises 201 and 249; Yogodzinski et al., 2015; Yogodzinski et al., 2017). These Aleutian lavas have a characteristic trace element signature of very high Sr/Y (up to 400; Figure S4), high to very high Sr contents (1250–2500 µg/g; Figure S4), strongly fractionated but variable REE patterns (La_N/Yb_N 7–41) with large variation in LREE contents. The radiogenic isotope composition of western Aleutian lavas suggests negligible sediment involvement with very low $^{87}Sr/^{86}Sr$ (<0.7029), radiogenic $^{143}Nd/^{144}Nd$ (>0.51305) and MORB-like $\delta^{18}O$ (Yogodzinski et al., 2015; Yogodzinski et al., 2017). Crustal processes are negligible in the western Aleutian arc. In the Western Cones and Komandorsky Straits, evolved (Mg# <55) lavas are absent altogether, indicating that very little melt evolution through fractional crystallisation has happened to these seafloor samples emplaced on oceanic crust. This also means that there is no evolved magma component available for magma mixing, and hence the primitive andesites and rhyodacites are a primary feature of magmas generated though subduction of the 50–60 Ma Pacific plate.

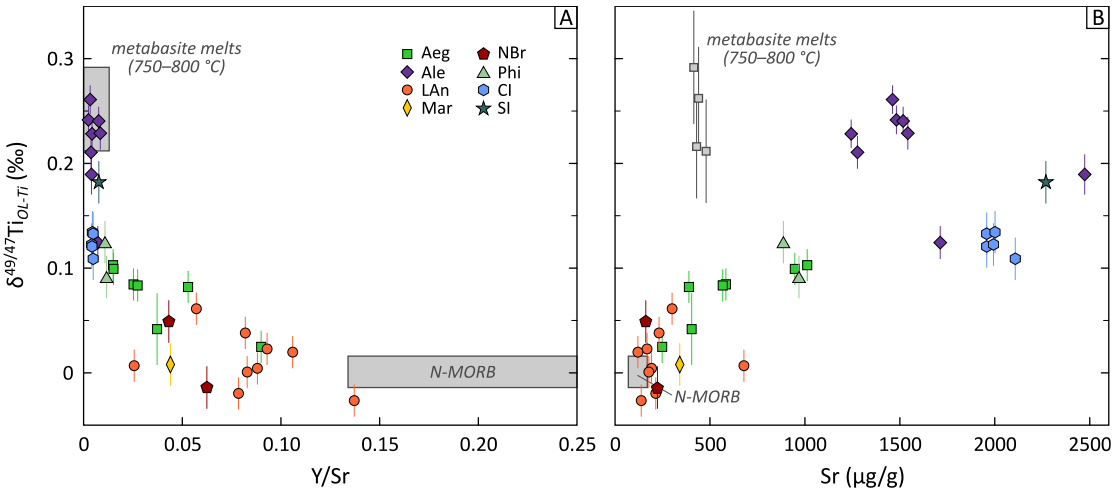

Figure S4. *Titanium isotope composition of primitive arc lavas (Mg# ≥60) versus Y/Sr and Sr content (see supplementary Dataset 2). The trace element composition of N-MORB is from Arevalo and McDonough (2010); for N-MORB $\delta^{49/47}$Ti see Figure 1 in the main text. Titanium isotope composition of metabasite melts at 750–800 °C is taken from the models shown in Figure 2 in the main text; trace element data from Carter et al. (2015) and Sisson and Kelemen (2018). Location abbreviations: Aeg – Aegean arc; Ale – Aleutian arc; LAn – Lesser Antilles arc; Mar – Mariana arc; NBr – New Britain arc; Phi – Philippines arc; CI – Cook Island (Austral Volcanic Zone, Chile); SI – Solander Islands (New Zealand).*

Lesser Antilles arc

Westward subduction of the Atlantic lithosphere under the Caribbean plate gives rise to volcanism along the ca. 750 km long Lesser Antilles arc. Radiogenic isotope and trace element data show a general decrease in the amount of subducted sediment in Lesser Antilles arc lavas from the north to the south (e.g., Macdonald et al., 2000). Most of the Lesser Antilles samples measured in this study come from the southern islands St. Vincent, Bequia (the largest of the Grenadines), and Grenada. The samples include several highly magnesian picrites (12.9–15.6 wt.% MgO, 45–47 wt.% SiO_2) from St. Vincent (Robertson, 2002) and one high-La/Y picrite from Grenada (Thirlwall et al., 1996). Three samples from Bequia (Camejo-Harry et al., 2018) and a single sample from Saba, the northernmost active volcano of the Lesser Antilles arc, are more typical primitive arc basalts (50–52 wt.% SiO_2). All samples from these southern volcanic centres have flat HREE-patterns, low Sr/Y (mostly <20; Figure S4), and low Sr/Nd (mostly <30). Radiogenic isotope systematics of Lesser Antilles lavas reflect both the contribution of subducted sediment to the mantle source, as well as assimilation of sediments embedded in the Caribbean crust on which the volcanic edifices are built (e.g., Bezard et al., 2014; Rojas-Agramonte et al., 2017). Neodymium isotopes in the studied samples are relatively unradiogenic ($^{143}Nd/^{144}Nd$ = 0.51293–0.51300) with the exception of the high-La/Y picrite from Grenada and one Bequia sample that have notably less radiogenic Nd isotope compositions. As such, the Lesser Antilles samples do not share the geochemical signature often attributed to slab melting (e.g., high Sr/Y; Defant and Drummond, 1990) that is shown by many other new sample suites in this study.

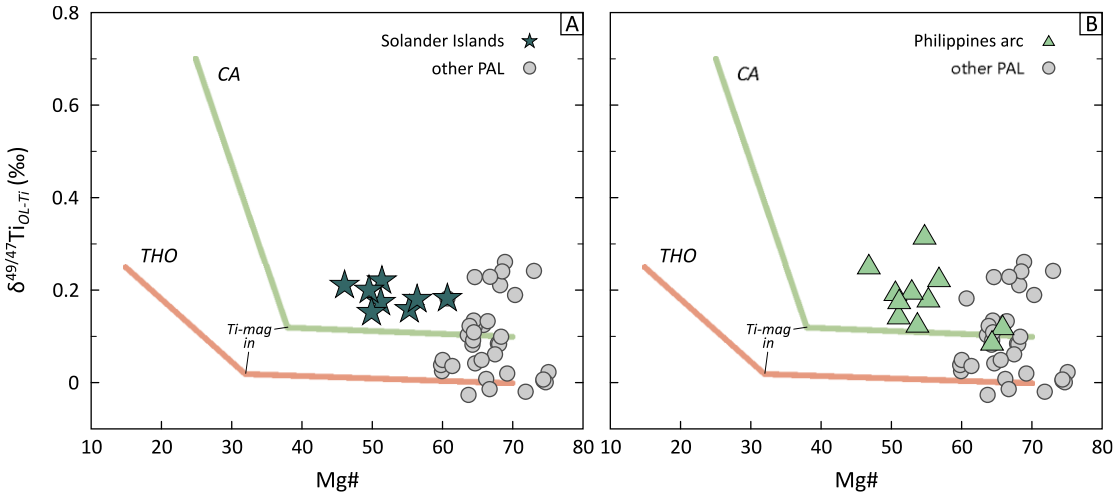

Figure S5. *Titanium isotope composition of Solander Islands (A) and Philippines arc (B) samples as a function of Mg#; other primitive arc lavas (PAL; Mg# ≥60) shown for comparison. The calc-alkaline (CA) and tholeiitic (THO) differentiation trends are based on the Aegean arc and Kermadec–New Britain arc data, respectively (see Figure 3 in the main text).*

Philippines arc

Miocene to Pleistocene volcanic rocks exposed on Mindanao, Philippines, are related to the incipient (since ca. 7 Ma) westward subduction of Philippines Sea Plate oceanic lithosphere. In addition to basalts with a normal island arc geochemical signature there are several occurrences of more silica-rich lavas with a characteristic trace element signature of high Sr contents (generally >800 µg/g), high Sr/Nd (generally >50), high Sr/Y (>60), and fractionated REE patterns. We include 11 Pleistocene lavas from the Surigao peninsula (Macpherson et al., 2006) that display a wide range in SiO_2 content (58–70) and Mg# (50–65), of which two samples are considered to be primitive (Mg# ≥60). On the basis of their distinctive trace element patterns, Sajona et al. (1993) designated such samples from Mindanao to be slab melts, but this interpretation was questioned based on Sr and Os isotope compositions of these lavas that are distinct from the subducting oceanic crust of the Philippines Sea Plate (Dreher et al., 2005; Macpherson et al., 2006). An alternative explanation for the characteristic trace element pattern of the Mindanao samples is derivation from a normal primitive arc basalt through fractional crystallisation of a garnet-rich assemblage in the upper mantle (Macpherson et al., 2006; Coldwell et al., 2011). An Fe-Ti oxide mineral was not considered to be a crystallising phase and removal of garnet and pyroxene will not cause notable change in $\delta^{49/47}Ti$ (see section 1 of the supplementary material), but also ca. 17 wt.% of amphibole is deemed to be present in the fractionating mineral assemblage (Macpherson et al., 2006). As there are, at present, no solid constraints on the magnitude of Ti isotope fractionation between amphibole and melt, it is not possible to model the Ti isotope effects of such a fractional crystallisation process. More evolved Surigao lavas (Mg# <60) do show somewhat higher $\delta^{49/47}Ti$ than primitive Surigao lavas (Figure S5b), suggesting a possible amphibole signature. The two primitive Surigao lavas with Mg# in near-equilibrium with mantle peridotite (Mg# ca. 65), however, show $\delta^{49/47}Ti$ clearly offset from N-MORB (Figure S5b), suggesting that this is a primary signature and not the result of fractional crystallisation.

Cook Island

Cook Island is the southernmost volcanic centre in the Andean Austral Volcanic Zone (49–54°S), Chile, where it results from the oblique subduction of young (ca. 25 Ma) oceanic crust of the Antarctic plate under the Scotia plate (Futa and Stern, 1988; Stern and Kilian, 1996). Its volcanic products are relatively homogeneous andesitic dome lavas (56–61 wt.% SiO_2) with invariably high Mg#. Stern and Kilian (1996) note that Cook Island andesites show little evidence for magma mixing and crustal contamination. As shown in Figure S4, the andesites have very high Sr contents (ca. 2000 µg/g; Figure S4) and Sr/Y (200–250), high Sr/Nd (54–61), and the most radiogenic Nd isotope compositions and lowest $^{87}Sr/^{86}Sr$ observed in the Andean subduction zone, with values that overlap

with MORB (this study; Stern and Kilian, 1996). In addition, O isotope systematics suggest that Cook Island andesites are in equilibrium with mantle wedge peridotite with negligible interaction with the crust (Bindeman et al., 2005). In all, Cook Island andesites are regarded as an example of lavas influenced by slab melting (e.g., Defant and Drummond, 1990; Yogodzinski et al., 2001).

Solander Islands

Solander Island and Little Solander Island are located on thin continental crust (<30 km thickness) about 40 km south of the New Zealand South Island, where volcanism results from the eastward subduction of the Australian plate beneath the Pacific plate. The samples included in this study are (trachy-)andesitic lavas with 58–62 wt.% SiO_2 and Mg# 46–64 described in detail in Foley et al. (2013). Only a single Solander Islands sample is considered primitive (Mg# 60.7). Fractional crystallization of plagioclase and amphibole, but not garnet, is thought to be the main process that controls the range in Mg# displayed by the Solander Islands lavas (Foley et al., 2013). There is, however, no evidence for fractional crystallization of titanomagnetite and, as a result, $\delta^{49/47}$Ti shows no correlation with Mg# and is invariable at 0.18–0.22‰ (Figure S5a). The Solander Islands lavas are characterised by high Sr/Y (80–130), high to very high Sr contents (1000–2500 µg/g; Figure S4), and primitive, MORB-like Sr–Nd isotope compositions (Foley et al., 2013). The radiogenic isotope systematics and absence of a ^{10}Be anomaly rule out significant assimilation of the Mesozoic continental basement and significant involvement of subducted sediments (Foley et al., 2014). The geochemical signature of the Solander Islands lavas reflects an important contribution of partial melt of the subducting slab in their source (Reay and Parkinson, 1997; Foley et al., 2013; Foley et al., 2014).

4. A quick word on trace elements

Figure S6 shows $\delta^{49/47}$Ti of the primitive arc lavas *versus* their Ti and Nb anomalies. A negative Nb–Ta anomaly is one of the hallmarks of subduction zone magmas (e.g., Gill, 1981), but can be explained by both slab-to-mantle wedge mass transfer by a rutile-saturated slab melt, or an aqueous fluid with negligible solubility for these elements. All primitive arc lavas studied here display the characteristic negative Nb anomaly, which is expressed as N-MORB (Gale et al., 2013) normalised Nb/Th <1 in Figure S6b. Samples with unfractionated $\delta^{49/47}$Ti, such as most of the Lesser Antilles samples, have a clear negative Nb anomaly but show no Ti isotope evidence for a slab melt contribution. Hence, in these cases it appears that aqueous fluids are the dominant medium for mass transport and that the negative Nb anomaly results from the very low solubility of Nb in even highly saline fluids (Keppler, 2017; Rustioni et al., 2021). Primitive arc lavas with a higher silica content, however, display a combination of elevated $\delta^{49/47}$Ti and low Nb/Th that is consistent with slab melts as the main medium for mass transfer from the slab. The primitive rhyodacites from the western Aleutian arc have $\delta^{49/47}$Ti and Nb/Th that overlap with low-degree slab melts (Sisson and Kelemen, 2018). Negative Nb anomalies by themselves are, therefore, no conclusive signature for either aqueous fluids or slab melts.

Primitive arc lavas with elevated $\delta^{49/47}$Ti also display an increasingly strong negative Ti anomaly, which is expressed as N-MORB normalised Ti/Eu in Figure 5a. These samples form a sublinear trend towards the composition of hydrous metabasite partial melts generated at 750–800 °C, which also have a negative Ti anomaly (Sisson and Kelemen, 2018). In contrast to the Nb anomaly that was present in all primitive arc lavas studies here, samples without elevated $\delta^{49/47}$Ti do not display a pronounced negative Ti anomaly. This suggests that slab fluids do not readily cause pronounced fractionation between Eu and Ti as both elements have relatively low solubility in aqueous fluids (Rustioni et al., 2021).

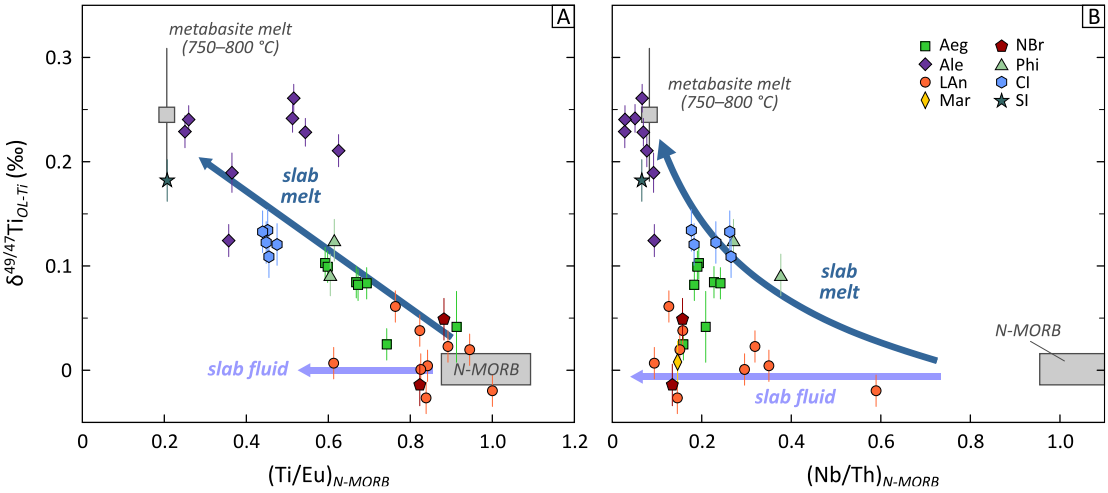

Figure S6. *Titanium isotope composition versus Ti anomaly (expressed as* $[Ti/Eu]_{N\text{-}MORB}$ *in panel A) and Nb anomaly (expressed as* $[Nb/Th]_{N\text{-}MORB}$ *in panel B). The trace element composition of N-MORB is from Arevalo and McDonough (2010); for N-MORB* $\delta^{49/47}Ti$ *see Figure 1 in the main text. Titanium isotope composition of metabasite melts at 750–800 °C is from models shown in Figure 2 in the main text; trace element data from Sisson and Kelemen (2018). The blue arrows represent schematic trends for the addition of slab fluids and slab melts.*

REFERENCES

Aarons, S.M., Dauphas, N., Blanchard, M., Zeng, H., Nie, N.X., Johnson, A.C., Greber, N.D., Hopp, T., 2021. Clues from ab initio calculations on titanium isotopic fractionation in tholeiitic and calc-alkaline magma series. ACS earth and space chemistry 5, 2466-2480.

Aarons, S.M., Reimink, J.R., Greber, N.D., Heard, A.W., Zhang, Z., Dauphas, N., 2020. Titanium isotopes constrain a magmatic transition at the Hadean-Archean boundary in the Acasta Gneiss Complex. Science Advances 6, eabc9959.

Anguelova, M., Fehr, M.A., Takazawa, E., Schönbächler, M., 2022. Titanium isotope heterogeneity in the Earth's mantle: a case study of the Horoman peridotite massif. Geochim. Cosmochim. Acta 335, 356-368.

Arevalo, R., McDonough, W.F., 2010. Chemical variations and regional diversity observed in MORB. Chem. Geol. 271, 70-85.

Auzanneau, E., Schmidt, M., Vielzeuf, D., D Connolly, J., 2010. Titanium in phengite: a geobarometer for high temperature eclogites. Contrib. Mineral. Petrol. 159, 1-24.

Bezard, R., Davidson, J.P., Turner, S., Macpherson, C.G., Lindsay, J.M., Boyce, A.J., 2014. Assimilation of sediments embedded in the oceanic arc crust: myth or reality? Earth Planet. Sci. Lett. 395, 51-60.

Bindeman, I., Eiler, J., Yogodzinski, G., Tatsumi, Y., Stern, C., Grove, T., Portnyagin, M., Hoernle, K., Danyushevsky, L., 2005. Oxygen isotope evidence for slab melting in modern and ancient subduction zones. Earth Planet. Sci. Lett. 235, 480-496.

Camejo-Harry, M., Melekhova, E., Blundy, J., Attridge, W., Robertson, R., Christopher, T., 2018. Magma evolution beneath Bequia, Lesser Antilles, deduced from petrology of lavas and plutonic xenoliths. Contrib. Mineral. Petrol. 173, 1-26.

Carter, L.B., Skora, S., Blundy, J., De Hoog, J., Elliott, T., 2015. An experimental study of trace element fluxes from subducted oceanic crust. J. Petrol. 56, 1585-1606.

Coldwell, B., Adam, J., Rushmer, T., Macpherson, C., 2011. Evolution of the East Philippine Arc: experimental constraints on magmatic phase relations and adakitic melt formation. Contrib. Mineral. Petrol. 162, 835-848.

Defant, M.J., Drummond, M.S., 1990. Derivation of some modern arc magmas by melting of young subducted lithosphere. Nature 347, 662-665.

Deng, Z., Chaussidon, M., Savage, P., Robert, F., Pik, R., Moynier, F., 2019. Titanium isotopes as a tracer for the plume or island arc affinity of felsic rocks. Proceedings of the National Academy of Sciences 116, 1132-1135.

Deng, Z., Moynier, F., Sossi, P., Chaussidon, M., 2018. Bridging the depleted MORB mantle and the continental crust using titanium isotopes. Geochemical Perspectives Letters 9, 11-15.
Dreher, S.T., Macpherson, C.G., Pearson, D.G., Davidson, J.P., 2005. Re-Os isotope studies of Mindanao adakites: Implications for sources of metals and melts. Geology 33, 957-960.
Druitt, T.H., Edwards, L., Mellors, R., Pyle, D., Sparks, R., Lanphere, M., Davies, M., Barreirio, B., 1999. Santorini volcano, London.
Elburg, M.A., Smet, I., De Pelsmaeker, E., 2014. Influence of source materials and fractionating assemblage on magmatism along the Aegean Arc, and implications for crustal growth. Geological Society, London, Special Publications 385, 137-160.
Foley, F.V., Pearson, N.J., Rushmer, T., Turner, S., Adam, J., 2013. Magmatic evolution and magma mixing of Quaternary adakites at Solander and Little Solander Islands, New Zealand. J. Petrol. 54, 703-744.
Foley, F.V., Turner, S., Rushmer, T., Caulfield, J.T., Daczko, N.R., Bierman, P., Robertson, M., Barrie, C.D., Boyce, A.J., 2014. ^{10}Be, ^{18}O and radiogenic isotopic constraints on the origin of adakitic signatures: a case study from Solander and Little Solander Islands, New Zealand. Contrib. Mineral. Petrol. 168, 1-28.
Futa, K., Stern, C.R., 1988. Sr and Nd isotopic and trace element compositions of Quaternary volcanic centers of the southern Andes. Earth Planet. Sci. Lett. 88, 253-262.
Gale, A., Dalton, C.A., Langmuir, C.H., Su, Y., Schilling, J.G., 2013. The mean composition of ocean ridge basalts. Geochem. Geophys. Geosyst. 14, 489-518.
Ghiorso, M.S., Hirschmann, M.M., Reiners, P.W., Kress III, V.C., 2002. The pMELTS: A revision of MELTS for improved calculation of phase relations and major element partitioning related to partial melting of the mantle to 3 GPa. Geochem. Geophys. Geosyst. 3, 1-35.
Gill, J., 1981. Orogenic andesites and plate tectonics. Springer, Berlin.
Greber, N.D., Dauphas, N., Bekker, A., Ptáček, M.P., Bindeman, I.N., Hofmann, A., 2017a. Titanium isotopic evidence for felsic crust and plate tectonics 3.5 billion years ago. Science 357, 1271-1274.
Greber, N.D., Dauphas, N., Puchtel, I.S., Hofmann, B.A., Arndt, N.T., 2017b. Titanium stable isotopic variations in chondrites, achondrites and lunar rocks. Geochim. Cosmochim. Acta 213, 534-552.
Greber, N.D., Pettke, T., Vilela, N., Lanari, P., Dauphas, N., 2021. Titanium isotopic compositions of bulk rocks and mineral separates from the Kos magmatic suite: Insights into fractional crystallization and magma mixing processes. Chem. Geol. 578, 120303.
Hoare, L., Klaver, M., Muir, D.D., Klemme, S., Barling, J., Parkinson, I.J., Lissenberg, C.J., Millet, M.-A., 2022. Empirical and experimental constraints on Fe-Ti oxide-melt titanium isotope fractionation factors. Geochim. Cosmochim. Acta 326, 253-272.
Hoare, L., Klaver, M., Saji, N.S., Gillies, J., Parkinson, I.J., Lissenberg, C.J., Millet, M.-A., 2020. Melt chemistry and redox conditions control titanium isotope fractionation during magmatic differentiation. Geochim. Cosmochim. Acta 282, 38-54.
Johnson, A.C., Aarons, S.M., Dauphas, N., Nie, N.X., Zeng, H., Helz, R.T., Romaniello, S.J., Anbar, A.D., 2019. Titanium isotopic fractionation in Kilauea Iki lava lake driven by oxide crystallization. Geochim. Cosmochim. Acta 264, 180-190.
Johnson, A.C., Zhang, Z.J., Dauphas, N., Rudnick, R.L., Foden, J.D., Toc, M., 2023. Redox and mineral controls on Fe and Ti isotopic fractionations during calc-alkaline magmatic differentiation. Geochim. Cosmochim. Acta.
Kay, R.W., 1978. Aleutian magnesian andesites: melts from subducted Pacific Ocean crust. J. Volcanol. Geotherm. Res. 4, 117-132.
Kelemen, P.B., Yogodzinski, G.M., Scholl, D.W., 2003. Along-strike variation in the Aleutian island arc: Genesis of high Mg# andesite and implications for continental crust. Inside the Subduction Factory, Geophys. Monogr. Ser 138, 223-276.
Keppler, H., 2017. Fluids and trace element transport in subduction zones. Am. Mineral. 102, 5-20.
Kessel, R., Ulmer, P., Pettke, T., Schmidt, M., Thompson, A., 2005. The water–basalt system at 4 to 6 GPa: Phase relations and second critical endpoint in a K-free eclogite at 700 to 1400 C. Earth Planet. Sci. Lett. 237, 873-892.
Klaver, M., Blundy, J.D., Vroon, P.Z., 2018. Generation of arc rhyodacites through cumulate-melt reactions in a deep crustal hot zone: Evidence from Nisyros volcano. Earth Planet. Sci. Lett. 497, 169-180.
Klaver, M., Davies, G.R., Vroon, P.Z., 2016. Subslab mantle of African provenance infiltrating the Aegean mantle wedge. Geology 44, 367-370.
Klaver, M., Lewis, J., Parkinson, I.J., Elburg, M.A., Vroon, P.Z., Kelley, K.A., Elliott, T., 2020. Sr isotopes in arcs revisited: tracking slab dehydration using $\delta^{88/86}$Sr and ^{87}Sr/^{86}Sr systematics of arc lavas. Geochim. Cosmochim. Acta 288, 101-119.

Klaver, M., Luu, T.-H., Lewis, J., Jansen, M.N., Anand, M., Schwieters, J., Elliott, T., 2021a. The Ca isotope composition of mare basalts as a probe into the heterogeneous lunar mantle. Earth Planet. Sci. Lett. 570, 117079.

Klaver, M., MacLennan, S.A., Ibañez-Mejia, M., Tissot, F.L.H., Vroon, P.Z., Millet, M.-A., 2021b. Reliability of detrital marine sediments as proxy for continental crust composition: The effects of hydrodynamic sorting on Ti and Zr isotope systematics. Geochim. Cosmochim. Acta 310, 221-239.

Klaver, M., Matveev, S., Berndt, J., Lissenberg, C.J., Vroon, P., 2017. A mineral and cumulate perspective to magma differentiation at Nisyros volcano, Aegean arc. Contrib. Mineral. Petrol. 172, 1-23.

Kommescher, S., Fonseca, R., Kurzweil, F., Thiemens, M., Münker, C., Sprung, P., 2020. Unravelling lunar mantle source processes via the Ti isotope composition of lunar basalts. Geochemical Perspectives Letters 13, 13-18.

Leitzke, F., Fonseca, R., Göttlicher, J., Steininger, R., Jahn, S., Prescher, C., Lagos, M., 2018. Ti K-edge XANES study on the coordination number and oxidation state of Titanium in pyroxene, olivine, armalcolite, ilmenite, and silicate glass during mare basalt petrogenesis. Contrib. Mineral. Petrol. 173, 1-17.

Macdonald, R., Hawkesworth, C.J., Heath, E., 2000. The Lesser Antilles volcanic chain: a study in arc magmatism. Earth-Science Reviews 49, 1-76.

Macpherson, C.G., Dreher, S.T., Thirlwall, M.F., 2006. Adakites without slab melting: high pressure differentiation of island arc magma, Mindanao, the Philippines. Earth Planet. Sci. Lett. 243, 581-593.

Mann, U., Schmidt, M.W., 2015. Melting of pelitic sediments at subarc depths: 1. Flux vs. fluid-absent melting and a parameterization of melt productivity. Chem. Geol. 404, 150-167.

Martin, L.A., Hermann, J., 2018. Experimental phase relations in altered oceanic crust: implications for carbon recycling at subduction zones. J. Petrol. 59, 299-320.

Martindale, M., Skora, S., Pickles, J., Elliott, T., Blundy, J., Avanzinelli, R., 2013. High pressure phase relations of subducted volcaniclastic sediments from the west pacific and their implications for the geochemistry of Mariana arc magmas. Chem. Geol. 342, 94-109.

Millet, M.-A., Dauphas, N., 2014. Ultra-precise titanium stable isotope measurements by double-spike high resolution MC-ICP-MS. J. Anal. At. Spectrom. 29, 1444-1458.

Millet, M.-A., Dauphas, N., Greber, N.D., Burton, K.W., Dale, C.W., Debret, B., Macpherson, C.G., Nowell, G.M., Williams, H.M., 2016. Titanium stable isotope investigation of magmatic processes on the Earth and Moon. Earth Planet. Sci. Lett. 449, 197-205.

Nie, N.X., Dauphas, N., Alp, E.E., Zeng, H., Sio, C.K., Hu, J.Y., Chen, X., Aarons, S.M., Zhang, Z., Tian, H.-C., 2021. Iron, magnesium, and titanium isotopic fractionations between garnet, ilmenite, fayalite, biotite, and tourmaline: Results from NRIXS, ab initio, and study of mineral separates from the Moosilauke metapelite. Geochim. Cosmochim. Acta 302, 18-45.

O'Neill, H.S.C., Navrotsky, A., 1983. Simple spinels; crystallographic parameters, cation radii, lattice energies, and cation distribution. Am. Mineral. 68, 181-194.

Palme, H., O'Neill, H., 2014. Cosmochemical estimates of mantle composition, in: Holland, H.D., Turekian, K.K. (Eds.), Treatise on geochemistry (2nd edition). Elsevier, Oxford, pp. 1-39.

Reay, A., Parkinson, D., 1997. Adakites from Solander Island, New Zealand. New Zeal. J. Geol. Geophys. 40, 121-126.

Robertson, R.E., 2002. Volcanic geology of the pre-Soufriere rocks on St. Vincent, West Indies. University of the West Indies.

Rojas-Agramonte, Y., Williams, I.S., Arculus, R., Kröner, A., García-Casco, A., Lázaro, C., Buhre, S., Wong, J., Geng, H., Echeverría, C.M., 2017. Ancient xenocrystic zircon in young volcanic rocks of the southern Lesser Antilles island arc. Lithos 290, 228-252.

Rustioni, G., Audetat, A., Keppler, H., 2021. The composition of subduction zone fluids and the origin of the trace element enrichment in arc magmas. Contrib. Mineral. Petrol. 176, 51.

Rzehak, L.J., Kommescher, S., Kurzweil, F., Sprung, P., Leitzke, F.P., Fonseca, R.O., 2021. The redox dependence of titanium isotope fractionation in synthetic Ti-rich lunar melts. Contrib. Mineral. Petrol. 176, 1-16.

Rzehak, L.J.A., Kommescher, S., Hoare, L., Kurzweil, F., Sprung, P., Leitzke, F.P., Fonseca, R.O.C., 2022. Redox-dependent Ti stable isotope fractionation on the Moon: implications for current lunar magma ocean models. Contrib. Mineral. Petrol. 177, 1-20.

Sajona, F.G., Maury, R.C., Bellon, H., Cotten, J., Defant, M.J., Pubellier, M., 1993. Initiation of subduction and the generation of slab melts in western and eastern Mindanao, Philippines. Geology 21, 1007-1010.

Schmidt, M.W., Vielzeuf, D., Auzanneau, E., 2004. Melting and dissolution of subducting crust at high pressures: the key role of white mica. Earth Planet. Sci. Lett. 228, 65-84.

Sisson, T., Kelemen, P., 2018. Near-solidus melts of MORB + 4 wt% H_2O at 0.8–2.8 GPa applied to issues of subduction magmatism and continent formation. Contrib. Mineral. Petrol. 173, 1-23.

Skora, S., Blundy, J., 2010. High-pressure hydrous phase relations of radiolarian clay and implications for the involvement of subducted sediment in arc magmatism. J. Petrol. 51, 2211-2243.

Skora, S., Blundy, J.D., Brooker, R.A., Green, E.C., de Hoog, J., Connolly, J.A., 2015. Hydrous phase relations and trace element partitioning behaviour in calcareous sediments at subduction-zone conditions. J. Petrol. 56, 953-980.

Stern, C.R., Kilian, R., 1996. Role of the subducted slab, mantle wedge and continental crust in the generation of adakites from the Andean Austral Volcanic Zone. Contrib. Mineral. Petrol. 123, 263-281.

Syracuse, E.M., van Keken, P.E., Abers, G.A., 2010. The global range of subduction zone thermal models. Phys. Earth Planet. Inter. 183, 73-90.

Thirlwall, M., 1991. Long-term reproducibility of multicollector Sr and Nd isotope ratio analysis. Chemical Geology: Isotope Geoscience section 94, 85-104.

Thirlwall, M., Graham, A., Arculus, R., Harmon, R., Macpherson, C., 1996. Resolution of the effects of crustal assimilation, sediment subduction, and fluid transport in island arc magmas: Pb-Sr-Nd-O isotope geochemistry of Grenada, Lesser Antilles. Geochim. Cosmochim. Acta 60, 4785-4810.

Tirel, C., Gueydan, F., Tiberi, C., Brun, J.-P., 2004. Aegean crustal thickness inferred from gravity inversion. Geodynamical implications. Earth Planet. Sci. Lett. 228, 267-280.

van Hinsbergen, D.J.J., Hafkenscheid, E., Spakman, W., Meulenkamp, J., Wortel, R., 2005. Nappe stacking resulting from subduction of oceanic and continental lithosphere below Greece. Geology 33, 325-328.

Vanderkluysen, L., Volentik, A., Hernandez, J., Hunziker, J.C., Bussy, F., Principe, C., 2005. The petrology and geochemistry of lavas and tephras of Nisyros Volcano (Greece), in: Hunziker, J.C., Marini, L. (Eds.), The Geology, Geochemistry and Evolution of Nisyros Volcano (Greece). Implications for the Volcanic Hazards, Lausanne, pp. 79-99.

Wang, W., Huang, S., Huang, F., Zhao, X., Wu, Z., 2020. Equilibrium inter-mineral titanium isotope fractionation: Implication for high-temperature titanium isotope geochemistry. Geochim. Cosmochim. Acta 269, 540-553.

Williams, N.H., Fehr, M.A., Parkinson, I.J., Mandl, M.B., Schönbächler, M., 2021. Titanium isotope fractionation in solar system materials. Chem. Geol. 568, 120009.

Yogodzinski, G., Kay, R., Volynets, O., Koloskov, A., Kay, S., 1995. Magnesian andesite in the western Aleutian Komandorsky region: implications for slab melting and processes in the mantle wedge. Geol. Soc. Am. Bull. 107, 505-519.

Yogodzinski, G., Lees, J., Churikova, T., Dorendorf, F., Wöerner, G., Volynets, O., 2001. Geochemical evidence for the melting of subducting oceanic lithosphere at plate edges. Nature 409, 500-504.

Yogodzinski, G.M., Brown, S.T., Kelemen, P.B., Vervoort, J.D., Portnyagin, M., Sims, K.W., Hoernle, K., Jicha, B.R., Werner, R., 2015. The role of subducted basalt in the source of island arc magmas: evidence from seafloor lavas of the western Aleutians. J. Petrol. 56, 441-492.

Yogodzinski, G.M., Kelemen, P.B., Hoernle, K., Brown, S.T., Bindeman, I., Vervoort, J.D., Sims, K.W., Portnyagin, M., Werner, R., 2017. Sr and O isotopes in western Aleutian seafloor lavas: Implications for the source of fluids and trace element character of arc volcanic rocks. Earth Planet. Sci. Lett. 475, 169-180.

Young, E.D., Manning, C.E., Schauble, E.A., Shahar, A., Macris, C.A., Lazar, C., Jordan, M., 2015. High-temperature equilibrium isotope fractionation of non-traditional stable isotopes: Experiments, theory, and applications. Chem. Geol. 395, 176-195.

Zhao, X., Tang, S., Li, J., Wang, H., Helz, R., Marsh, B., Zhu, X., Zhang, H., 2020. Titanium isotopic fractionation during magmatic differentiation. Contrib. Mineral. Petrol. 175, 1-16.